

# T cells engineered against Dickkopf-1-A2 complex can be used to treat HLA-A2<sup>+</sup> solid and hematologic cancers

Received: 22 April 2025

Accepted: 4 February 2026

Published online: 16 February 2026

 Check for updates

Yufei Zhang<sup>1,6</sup>, Wei Xiong<sup>1,6</sup>, Jianfei Qian<sup>1,6</sup>, Rui Duan<sup>1,6</sup>, Qi Guo<sup>1</sup>, Qiang Wang<sup>1</sup>, Wei Wu<sup>1</sup>, Chuanchao Zhang<sup>1</sup>, Yabo Li<sup>1</sup>, Miao Xian<sup>1</sup>, Yong Lu<sup>1</sup>, Nestor F. Esnaola<sup>2</sup>, Jenny C. Chang<sup>3</sup>, Liuling Xiao<sup>1,4</sup>✉, Ling Zhong<sup>1,5</sup>✉ & Qing Yi<sup>1</sup>✉

Although chimeric antigen receptor (CAR)-T cells are promising effector cells to treat hematologic tumors, developing effective CAR-T cells for solid tumors remains challenging. Dickkopf-1 (DKK1) protein is widely expressed by human hematologic and solid tumors. Using the sequence of murine or humanized monoclonal antibody recognizing DKK1-A2 complexes (DKK1-P20 peptide in the context of HLA-A\*0201) that are detected on all examined HLA-A2<sup>+</sup> tumor samples but not normal tissues except tonsils, we generate DKK1-A2 CAR-T cells that specifically and effectively lyse HLA-A2- and DKK1-expressing tumor cells but not blood or bone marrow cells from HLA-A2<sup>+</sup> healthy donors. In xenograft models of human myeloma, pancreatic, lung, and breast cancers and patient-derived xenograft of pancreatic cancer, DKK1-A2 but not CD19 CAR-T cells effectively control or eradicate established tumors without detectable toxicities in NSG or human DKK1 and HLA-A2-transgenic mice. This study indicates that DKK1-A2 CAR-T cells may be used to treat human cancers.

Chimeric antigen receptor (CAR)-T cells have demonstrated remarkable clinical success in the treatment of hematologic tumors, especially those targeting antigens such as CD19 and BCMA<sup>1-6</sup>. These therapies have significantly advanced the management of blood cancers, including lymphomas, some forms of leukemia, and most recently multiple myeloma (MM)<sup>7</sup>. However, developing effective CAR-T cell therapies for solid tumors remains challenging<sup>8</sup>. Although some tumor antigens, such as Mucin-1<sup>9</sup>, Glypican-3<sup>10</sup> and Claudin 18.2<sup>11</sup> have been explored in research, identifying safe and effective antigens for CAR-T cell therapies for both hematologic and solid tumors continues to be a major hurdle<sup>12</sup>.

Dickkopf-1 (DKK1) is a secreted protein that acts as an antagonist of the Wnt/ $\beta$ -catenin signaling pathway<sup>13</sup>. DKK1 binds to LRP5/6 co-receptors on the cell surface, preventing them from interacting with Wnt proteins<sup>14,15</sup>. DKK1 overexpression has been observed in various cancers, including MM<sup>16</sup>, pancreatic cancer<sup>17</sup>, lung cancer<sup>18</sup>, breast cancer<sup>19</sup>, and hepatocellular cancer<sup>20</sup>. In MM, elevated DKK1 level leads to bone lesions and osteoporosis due to the imbalance in bone remodeling<sup>21</sup>. In certain tumors, DKK1 also promotes tumor progression by creating a microenvironment that supports cancer growth, affects immune response, and facilitates metastasis<sup>22,23</sup>. Conversely, DKK1 has limited expression in normal tissues, with the exception of

<sup>1</sup>Center for Translational Research in Hematological Malignancies, Houston Methodist Neal Cancer Center, Houston Methodist Research Institute, Houston, TX, USA. <sup>2</sup>Houston Methodist Neal Cancer Center, Houston Methodist Research Institute, and Surgical Oncology and Gastrointestinal Surgery, Department of Surgery, Houston Methodist Hospital, Houston, TX, USA. <sup>3</sup>Houston Methodist Academic Institute, Houston Methodist Hospital, Houston, TX, USA. <sup>4</sup>Present address: First Affiliated Hospital, School of Basic Medicine, Chongqing Medical University, Chongqing, China. <sup>5</sup>Present address: Genetic Diseases Key Laboratory of Sichuan Province, Department of Medical Genetics, Department of Laboratory Medicine, Sichuan Academy of Medical Sciences & Sichuan Provincial People's Hospital, School of Medicine, University of Electronic Science and Technology of China, Chengdu, Sichuan, China. <sup>6</sup>These authors contributed equally: Yufei Zhang, Wei Xiong, Jianfei Qian, Rui Duan. ✉e-mail: [xiaoliuling@cqmu.edu.cn](mailto:xiaoliuling@cqmu.edu.cn); [zhonglingr@126.com](mailto:zhonglingr@126.com); [qyi@houstonmethodist.org](mailto:qyi@houstonmethodist.org)

the placenta and testis<sup>24,25</sup>. This reciprocal expression makes DKK1 an attractive target for cancer immunotherapy<sup>26</sup>, particularly in developing CAR-T cell therapies for both MM and solid tumors.

To target DKK1 for cancer immunotherapy, we identified a DKK1 peptide, P20 (ALGGHPLLGV), that showed an excellent binding affinity to HLA-A\*0201 (for short, HLA-A2 or A2), which is a widely distributed HLA serotype found in 30–50% of the human population<sup>25,27</sup>. We developed a T cell receptor-like monoclonal antibody (C2) that recognizes DKK1-P20 peptide in the context of HLA-A2 molecules (hereafter, referred as DKK1-A2 complex)<sup>28</sup>. This C2 antibody can directly induce apoptosis in DKK1-A2 positive cancer cells and indirectly lyse DKK1-A2 positive cancer cells by mediating antibody-dependent cellular cytotoxicity and complement-dependent cytotoxicity. Furthermore, C2 antibody was therapeutic against established cancers in human xenograft mouse models. Notably, C2 antibody did not bind to or kill HLA-A2 positive blood or bone marrow cells in vitro, nor caused tissue damage in tumor-free or tumor-bearing HLA-A2-transgenic mice. The exceptional specificity and safety profile make the C2 antibody a promising candidate for developing CAR-T cell therapy.

In this study, we developed a DKK1-A2 CAR, incorporating the single-chain variable fragment (scFv) of C2 antibody along with 4-1BB and CD3 $\zeta$  costimulatory domains to generate human DKK1-A2 CAR-T cells. We hypothesized that this CAR-T cell therapy could effectively target HLA-A2 positive MM and a broad range of solid tumors, including pancreatic cancer, lung cancer, and breast cancers that express DKK1. Our results clearly showed that DKK1-A2 CAR-T cells have a strong anti-tumor effect in vitro and in vivo against established hematologic and solid tumors with a favorable safety profile, and DKK1-A2 CAR-T cells may be a promising therapeutic tool to treat DKK1-A2 positive human cancers.

## Results

### DKK1 and DKK1-A2 expression profiles in different cancers and normal tissues

To evaluate *DKK1* expression in hematologic tumors, three gene sequencing datasets from myeloma<sup>29</sup>, lymphoma<sup>30</sup>, and leukemia<sup>31</sup> were analyzed. *DKK1* mRNA was highly expressed in many hematologic tumors, particularly in MM and acute leukemia originated from B cells (Fig. 1a). MM exhibited the highest *DKK1* expression among various hematologic tumors, reaching up to around 70-fold higher than plasma cells from healthy donors (Fig. 1a). To determine *DKK1* expression in solid tumors, its gene expression profiles across all tumor samples from GEPIA2 database<sup>32</sup> were utilized for analysis (Fig. 1b). Most TCGA solid tumor types highly expressed *DKK1* mRNA compared to paired normal tissues, particularly in pancreatic adenocarcinoma (PAAD)<sup>33</sup> that expressed more than 90-fold *DKK1* than normal pancreatic tissues (Fig. 1b). Pancreatic ductal adenocarcinoma (PDAC) patients with a higher expression of *DKK1* had inferior overall and disease-free survivals than patients with a lower expression of *DKK1* (Fig. 1c, d). Similarly, poor prognosis was also found in other solid tumors with higher *DKK1* expression, such as lung adenocarcinoma (LUAD), lung squamous cell carcinoma (LUSC), stomach adenocarcinoma (STAD), and head and neck squamous cell carcinoma (HNSC) (Supplementary Fig. 1a–d). Oncomine datasets were used to validate *DKK1* expression in tumor types of interest. PDAC<sup>34</sup>, non-small cell lung cancer (NSCLC)<sup>35</sup>, and triple negative breast cancer (TNBC)<sup>36</sup> exhibited higher *DKK1* mRNA expression compared to normal tissues (Fig. 1e). Immunohistochemistry was utilized to determine the expression of DKK1 protein and DKK1-A2 complex by tumor tissues. Our results showed that DKK1 protein was not detected in normal pancreatic, lung, or breast tissues from HLA-A2 positive donors (Fig. 1f). However, all tumor tissues from 10 randomly selected PDAC (Fig. 1g), NSCLC (Fig. 1h), or TNBC (Fig. 1i) patients expressed high levels of DKK1 protein. Among these patients, 4/10, 6/10, and 6/10, respectively, are

HLA-A2 positive, and tumor samples from all these HLA-A2 positive patients expressed DKK1-A2 complexes stained by C2 antibody (Fig. 1g–i). Similarly, tissue array analysis showed that all of 40 NSCLC tumor tissues but none of 10 normal lung tissues highly expressed DKK1 protein, and 8 out of the 40 NSCLC patients were HLA-A2 positive and stained positive with C2 antibody (Supplementary Fig. 1e). One DKK1 negative and HLA-A2 positive TNBC sample was included and stained negative for C2 antibody (Supplementary Fig. 1f). Immunohistochemistry staining of DKK1, HLA-A2 and DKK1-A2 complex was controlled by isotype controls (Supplementary Fig. 1g). Together, these data revealed that DKK1 protein is highly expressed by multiple tumors, its expression is associated with poor survival of some cancer patients, and all HLA-A2-positive tumors express high levels of DKK1-A2 complexes recognized by C2 antibody.

### DKK1-A2 CAR-T cells display strong anti-tumor activity in vitro

As C2 antibody recognizes DKK1-A2 complex on tumor cells but not normal tissues, we generated DKK1-A2 CAR-T cells to target tumor cells that express DKK1-A2 complex (Fig. 2a). DKK1-A2 CAR consisted of the scFv derived from C2 antibody, 4-1BB, and CD3 $\zeta$  intracellular domains. Herein, both of murine C2 antibody (mC2) and humanized C2 antibody (hC2) were used to generate DKK1-A2 CAR-T cells. If not otherwise specified, DKK1-A2 CAR-T cells refer to mC2 CAR-T cells. CD19 CAR-T cells were generated and utilized as a control. Enhanced green fluorescent protein (eGFP) was co-expressed with CAR to track CAR-T cells (Fig. 2b). The average transduction efficiency of activated human T cells was around 70% (Fig. 2c). To evaluate the anti-tumor activity of DKK1-A2 CAR-T cells, MM, PDAC, NSCLC, and TNBC cell lines were used. As DKK1 is widely expressed by the tumor cell lines, C2 antibody could bind to HLA-A2 positive tumor cell lines, including JeKo-1, U266, KMS-26, CFPAC-1, PANC-1, NCI-H441, and MDA-MB-231 (Fig. 2d), but not HLA-A2 negative tumor cell lines (Supplementary Fig. 2a). CD19 expression on the tumor cells was also determined by flow cytometry. JeKo-1 and Daudi but not MM cell lines expressed CD19 (Supplementary Fig. 2b). The proliferation of CAR-T cells was corroborated by Celltrace dilution assay, as DKK1-A2 CAR-T cells exhibited a strong proliferation in response to HLA-A2 positive tumor cells compared to CD19 or control CAR-T cells (Fig. 2e). Cytolytic activity of DKK1-A2 CAR-T cells against tumor cells was determined by a firefly luciferase (Luc)-based cytotoxicity assay. DKK1-A2 CAR-T cells significantly lysed HLA-A2 positive tumor cells in a dose-dependent manner (Fig. 2f). We also assessed the anti-tumor activity of DKK1-A2 CAR-T cells against HLA-A2-transduced tumor cell lines (Supplementary Fig. 2c) and observed significant cytolytic activity and enhanced proliferation of DKK1-A2 CAR-T cells against MM.1S-A2, KMS-12-BM-A2, or PL45-A2 tumor cells (Supplementary Fig. 2d, e). DKK1-knockout (KO) JeKo-1 cells were generated by CRISPR-Cas9 (Supplementary Fig. 2f) and cytolytic activity and proliferation of DKK1-A2 CAR-T cells were not observed against JeKo-1-KO cells (Supplementary Fig. 2g, h). The anti-tumor activity of DKK1-A2 CAR-T cells was further supported by IFN- $\gamma$  and TNF- $\alpha$  production by both CD4<sup>+</sup> and CD8<sup>+</sup> DKK1-A2 CAR-T cells in their co-culture with tumor cell lines by flow cytometry (Fig. 2g, h) and ELISA (Supplementary Fig. 2i, j). Overall, DKK1-A2 CAR-T cells exhibit strong target-specific anti-tumor activity against HLA-A2 positive tumor cells in vitro.

### Therapeutic efficacy of DKK1-A2 CAR-T cells in human MM xenograft models

To evaluate the in vivo anti-tumor effects of DKK1-A2 CAR-T cells, we first established and used MM xenograft tumor models. U266 MM cells were implanted intravenously into NSG mice. Four weeks later, mice were infused intravenously with either control, CD19, or DKK1-A2 CAR-T cells, and tumor burden, determined by measuring the amounts of human immunoglobulin lambda (Ig $\lambda$ ) chain secreted by MM cells, was monitored weekly by ELISA (Fig. 3a). DKK1-A2 CAR-T cells effectively

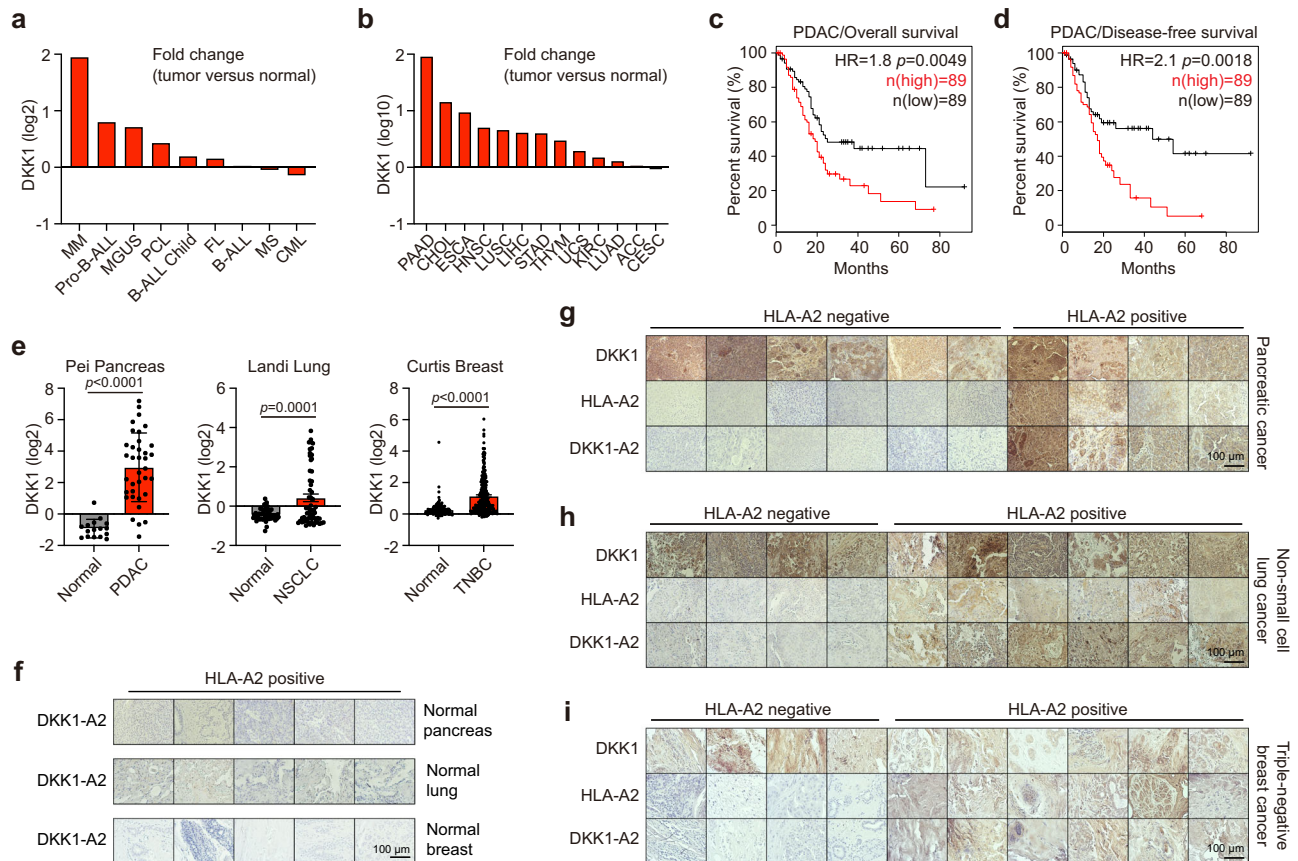


**Fig. 1 | Expression profiles of DKK1 and DKK1-A2 complex in human tumors and normal tissues.**

**a** Expression of *DKK1* mRNA across hematologic tumors was ranked, and datasets of GSE13591, GSE2350, and GSE13159 from Oncomine database were used. MM (multiple myeloma), Pro-B-ALL (Pro-B cell acute lymphoblastic leukemia), MGUS (monoclonal gammopathy of undetermined significance), PCL (primary plasma cell leukemia), B-ALL Child (B-Cell acute lymphoblastic leukemia in children), FL (follicular lymphoma), B-ALL (B-cell acute lymphoblastic leukemia), MS (myelodysplastic syndrome), CML (chronic myeloid leukemia). **b** Expression of *DKK1* mRNA across TCGA solid tumors compared to paired normal tissues was ranked in GEPIA2 database. PAAD (pancreatic adenocarcinoma), CHOL (cholangiocarcinoma), ESCA (esophageal carcinoma), HNSC (head and neck squamous cell carcinoma), LUSC (lung squamous cell carcinoma), LIHC (liver hepatocellular carcinoma), STAD (stomach adenocarcinoma), THYM (thymoma), UCS (uterine carcinosarcoma), KIRC (kidney renal clear cell carcinoma), LUAD (lung adenocarcinoma), ACC (adrenocortical carcinoma), CESC (cervical squamous cell carcinoma and endocervical adenocarcinoma). **c, d** Overall and disease-free survival of

pancreatic cancer patients with *DKK1*-high versus *DKK1*-low expression in GEPIA2 database. The top 50% patients with higher expressions of *DKK1* were defined as *DKK1*-high, and the rest were defined as *DKK1*-low patients. Hazards ratio and *p* value are demonstrated. Cox proportional hazards regression was used. **e** Solid tumor datasets of Pei Pancreas (GSE16515, normal *n* = 16, tumor *n* = 36), Landi Lung (GSE10072, normal *n* = 49, tumor *n* = 58) and Curtis Breast (EGAS00000000083, normal *n* = 144, tumor *n* = 250) from Oncomine database showing the expression of *DKK1* mRNA in tumor and paired normal tissues. Two-tailed Student's *t*-test was used. **f** Immunohistochemistry staining of DKK1-A2 complex on normal pancreatic, lung, or breast tissues from 5 randomly selected HLA-A2 positive donors. **g–i** Immunohistochemistry staining of DKK1, HLA-A2, and DKK1-A2 complex of 10 randomly selected HLA-A2 positive or negative PDAC, NSCLC, and TNBC tumor tissues. The independent experiments were repeated three times, and representative images are shown for immunohistochemistry staining. Data shown as mean  $\pm$  SEM. Source data are provided as a Source data file.

controlled U266 cell growth, and all mice remained alive at 7 weeks post CAR-T cell infusion, while CD19 CAR-T cells failed to do so (Fig. 3b, c). The body weight of all treated mice was not significantly changed after CAR-T cell therapy (Fig. 3d). Similar data were obtained from DKK1-A2 positive and CD19 negative KMS-26<sup>37</sup> MM model (Supplementary Fig. 3a–d).

### Therapeutic efficacy of DKK1-A2 CAR-T cells in human solid tumor xenograft models

We then assessed the anti-tumor efficacy of DKK1-A2 CAR-T cells against human solid tumors in their xenograft mouse models. First, firefly luciferase-transduced CFPAC-1 PDAC tumor cells were implanted subcutaneously 1 week before CAR-T cells infusion, and tumor volume and bioluminescence intensity were monitored weekly (Supplementary Fig. 3e). DKK1-A2 CAR-T cells effectively controlled tumor growth, evidenced by bioluminescence and survival rate, and body weight was not significantly changed after CAR-T cell therapy (Supplementary Fig. 3f–i).

More importantly, we developed and used a PDAC orthotopically xenografted model by implanting CFPAC-1-Luc tumor cells into mice pancreas<sup>38</sup> (Fig. 3e). Again, DKK1-A2 CAR-T cells exhibited effective and safe anti-tumor activity, evidenced by bioluminescence, survival, and body weight monitoring (Fig. 3f–i). Second, we used a NSCLC metastatic model by injecting Luc-transduced NCI-H441 tumor cells intravenously into NSG mice (Fig. 3j). DKK1-A2 CAR-T cells significantly reduced metastatic tumor burden, and all DKK1-A2 CAR-T cell-treated mice achieved a superior survival rate. Body weight was decreased after control, and CD19 CAR-T cell therapy, mainly due to tumor progression, and body weight was not significantly changed after DKK1-A2 CAR-T cell therapy (Fig. 3k–n). Third, the anti-tumor efficacy of DKK1-A2 CAR-T cells was examined in orthotopic (Fig. 3o) and subcutaneous (Supplementary Fig. 3j) Luc-transduced MDA-MB-231 TNBC models. Again, DKK1-A2 CAR-T cell treatment effectively controlled MDA-MB-231 tumor growth and resulted in long-term survival in all mice in the orthotopic model. DKK1-A2 CAR-T cell therapy did not significantly

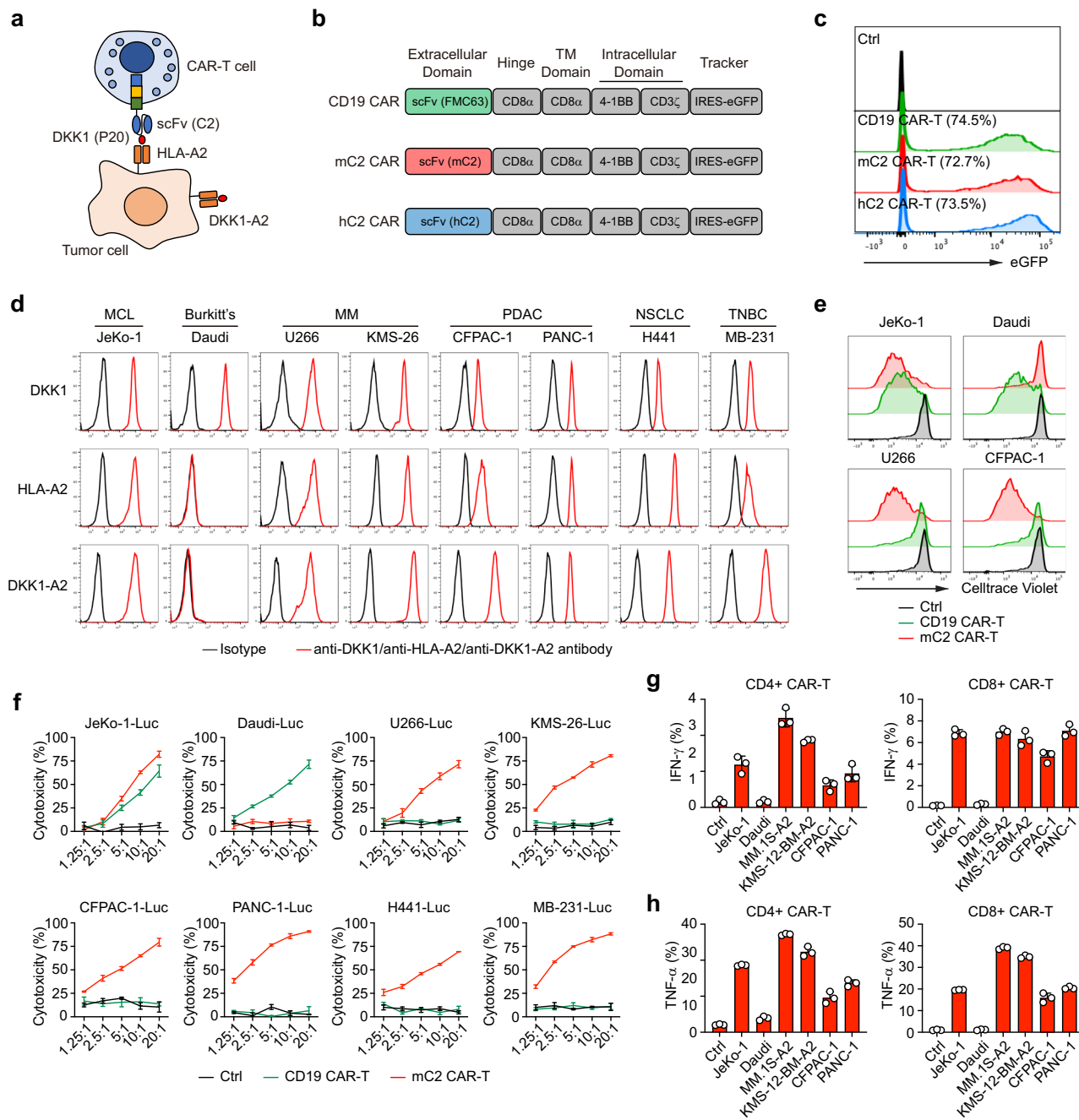


**Fig. 2 | In vitro cytolytic activity of DKK1-A2 CAR-T cells against human tumor cells.** **a** Schematic presentation showing the recognition of DKK1-A2 CAR-T cells and DKK1-A2 expressing tumor cells. **b** Schematic presentation showing DKK1-A2 and CD19 CAR constructs. **c** Percentage of CAR expressing T cells determined as eGFP positive T cells by flow cytometry analysis. **d** Expression of DKK1, HLA-A2 or DKK1-A2 complex by JeKo-1, Daudi, U266, KMS-26, CFPAC-1, PANC-1, NCI-H441 or MDA-MB-231 tumor cell lines determined by flow cytometry. **e** CAR-T cell proliferation measured by dilution of Celltrace Violet analyzed by flow cytometry. CAR-T cells were stained with Celltrace Violet and co-cultured with JeKo-1, Daudi, U266 or CFPAC-1 tumor cells at an E:T ratio of 1:1 for 72 h. **f** Cytotoxicity of

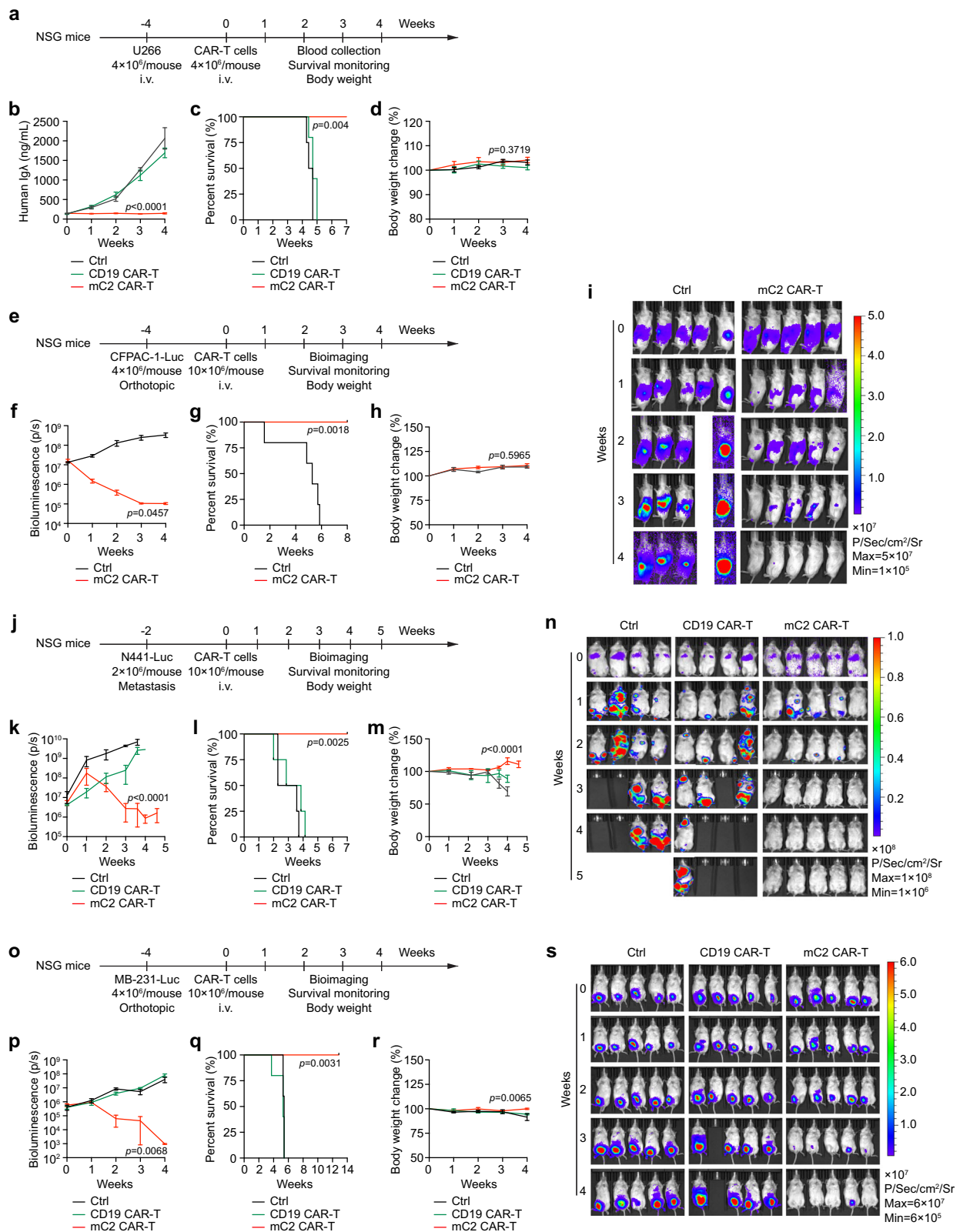
CAR-T cells determined by luciferase reporter assay. CAR-T cells were co-cultured with Luc-transduced JeKo-1, Daudi, U266, KMS-26, CFPAC-1, PANC-1, NCI-H441, or MDA-MB-231 tumor cells at indicated E:T ratios for 12 h.  $n = 3$ , technical replicates. **g, h** Percentages of IFN- $\gamma$  and TNF- $\alpha$  producing CD4 $^{+}$  or CD8 $^{+}$  CAR-T cells determined by intracellular cytokine staining. CAR-T cells were co-cultured with JeKo-1, Daudi, MM.1S-A2, KMS-12-BM-A2, CFPAC-1 or PANC-1 tumor cells at an E:T ratio of 1:1 overnight. In the experiments, CD19 CAR-T cells were used as a control.  $n = 3$ , technical replicates. Data shown as mean  $\pm$  SEM. Source data are provided as a Source data file.

affect the body weight of all mice (Fig. 3p–s). Similarly, DKK1-A2 CAR-T cells exhibited strong anti-tumor efficacy in the subcutaneous model (Supplementary Fig. 3k–n). Also, the TUNEL assay was performed in CFPAC-1 orthotopic, NCI-H441 metastatic, and MDA-MB-231 orthotopic models after CAR-T cell therapy. We observed CAR-T cell infiltration coupled with tumor apoptosis in the tumor tissues after DKK1-A2 CAR-T cell but not control or CD19 CAR-T cell treatment (Supplementary

Fig. 4a–c). In most of these studies, CD19 CAR-T cells were used as a control, and no anti-tumor effect was observed.

### Therapeutic efficacy of DKK1-A2 CAR-T cells in PDAC patient-derived xenograft model

Patient-derived xenograft (PDX) models effectively replicate the histology and genetic profile of the original patient tumors<sup>39</sup>. In



collaboration with our surgical oncologists, we obtained fresh tumor samples from 7 PDAC patients. Primary PDAC tumors were expanded in the flanks of NSG mice for 1–3 passages, allowing for greater expansion of tumor tissues<sup>40</sup> (Supplementary Fig. 5a, b). All primary PDAC tumor tissues expressed a high level of DKK1 protein, and DKK1-A2 complexes were detected in two HLA-A2 positive patients (PDAC #1 and #14; Fig. 4a). Proliferation of DKK1-A2 CAR-T cells was found in

their co-culture with PDAC #1 and #14 tumor cells but not with HLA-A2 negative PDAC cells (Fig. 4b). Celltrace Violet-labeled primary PDAC cells were co-cultured with control, CD19, or DKK1-A2 CAR-T cells for 3 days, and DKK1-A2 but not CD19 CAR-T cells eliminated nearly all HLA-A2 positive PDAC #1 tumor cells but not HLA-A2 negative PDAC #2 cells (Fig. 4c, d). Activation of DKK1-A2 CAR-T cells was also supported by higher levels of IFN- $\gamma$ , TNF- $\alpha$ , and Granzyme B production by both

**Fig. 3 | In vivo anti-tumor effects of DKK1-A2 CAR-T cells in human tumor xenograft mouse models.** **a** Schema of U266 MM xenograft model treated with CAR-T cells, **b** Tumor burden measured as the levels of human Ig $\lambda$  secreted by U266 cells. Blood was collected from U266 xenografted mice weekly and human Ig $\lambda$  in the serum was measured by ELISA, **c** Survival curve of U266 xenografted mice monitored daily before and post CAR-T cell infusion, and **d** Body weight change of U266 xenografted mice. Ctrl,  $n = 4$ ; CD19 CAR-T,  $n = 5$ ; mC2 CAR-T,  $n = 5$ ; biological replicates. **e** Schema of CFPAC-1-Luc PDAC orthotopic xenograft model treated with CAR-T cells, **f** Tumor burden shown as bioluminescence intensity of CFPAC-1-Luc PDAC orthotopic xenograft mice, **g** Survival curve of CFPAC-1-Luc PDAC orthotopically xenografted mice monitored daily before and post CAR-T cell infusion, **h** Body weight change of CFPAC-1-Luc PDAC orthotopic xenograft mice, and **i** Bioluminescence images of CFPAC-1-Luc PDAC orthotopic xenograft mice before and post CAR-T cell infusion. Ctrl,  $n = 5$ ; mC2 CAR-T,  $n = 5$ ; biological replicates. **j** Schema of NCI-H441-Luc NSCLC metastatic xenograft model treated with CAR-T cells infusion, **k** Bioluminescence intensity of NCI-H441-Luc NSCLC

metastatic xenograft mice, **l** Survival of NCI-H441-Luc NSCLC metastatic xenograft mice, **m** Body weight change of NCI-H441-Luc NSCLC metastatic xenograft mice, and **n** Bioluminescence images of NCI-H441-Luc NSCLC metastatic xenograft mice before and post CAR-T cell infusion. Ctrl,  $n = 4$ ; CD19 CAR-T,  $n = 4$ ; mC2 CAR-T,  $n = 5$ ; biological replicates. **o** Schema of MDA-MB-231-Luc TNBC orthotopic xenograft model treated with CAR-T cells, **p** Bioluminescence intensity of MDA-MB-231-Luc TNBC orthotopic xenograft mice, **q** Survival of MDA-MB-231-Luc TNBC orthotopic xenograft mice, **r** Body weight change of MDA-MB-231-Luc TNBC orthotopically xenografted mice, and **s** Bioluminescence images of MDA-MB-231-Luc TNBC orthotopic xenograft mice before and post-CAR-T cell infusion. Ctrl,  $n = 5$ ; CD19 CAR-T,  $n = 5$ ; mC2 CAR-T,  $n = 5$ ; biological replicates. Two-way ANOVA was used for bioluminescence, tumor volume, and body weight analyses (Two-tailed Student's *t*-test for CFPAC-1-Luc PDAC orthotopic xenograft model). Log-rank test was used for survival analysis. In most experiments, CD19 CAR-T cells were used as a control. Data shown as mean  $\pm$  SEM. Source data are provided as a Source data file.

CD4<sup>+</sup> and CD8<sup>+</sup> CAR-T cells in co-culture with PDAC #1 cells (Fig. 4e–g). To characterize primary and passage tumors of PDAC #1 PDX model, tumor tissues were digested and analyzed by flow cytometry (Supplementary Fig. 5c). Tumor cells were distinguished by carcinoembryonic antigen (CEA) staining. The primary and F3 passage tumors retained the same cellular composition, and nearly all the tumor cells were CEA, DKK1, and DKK1-A2 positive (Supplementary Fig. 5d). The results were also confirmed by immunohistochemistry staining with both low and high magnifications (Supplementary Fig. 5e, f). To evaluate the anti-tumor efficacy of DKK1-A2 CAR-T cells in the PDX model, expanded PDAC #1 tumor fragments were implanted subcutaneously into NSG mice, and CAR-T cells were infused intravenously 2 weeks post tumor inoculation (Fig. 4h). DKK1-A2 CAR-T cells effectively controlled tumor growth in vivo, and all mice achieved superior survival up to 8 weeks (Fig. 4i, j). Flow cytometry analysis showed that large numbers of circulating and resident (in spleen and bone marrow) DKK1-A2 but not control or CD19 CAR-T cells were detected at the end of the experiment (Fig. 4k). Collectively, these results showed that DKK1-A2 CAR-T cells are highly therapeutic against established hematologic and solid tumors, including primary tumors from HLA-A2 positive patients in vivo.

### Generation of DKK1-A2 CAR-T cells using a humanized C2 antibody

For future clinical application of DKK1-A2 CAR-T cells, we generated CAR-T cells with the scFv of the hC2 antibody constructed from the mC2 antibody. To compare the cytolytic activity of mC2 and hC2 CAR-T cells, U266, CFPAC-1, or primary PDAC tumor cells were used as targets and co-cultured with the CAR-T cells at different E:T ratios in a luciferase-based cytotoxicity assay. Both mC2 and hC2 CAR-T cells showed strong cytotoxicity against U266 and CFPAC-1 tumor cells (Fig. 5a, b), and both mC2 and hC2 CAR-T cells exhibited similar cytolytic activity against primary PDAC #1 cells at 24- or 72-h co-culture (Fig. 5c, d). To evaluate the anti-tumor activity of the CAR-T cells in vivo, U266, KMS-12-BM-A2, or MM.1S-A2 MM cell lines were utilized to establish xenograft models by tail vein injection into NSG mice (Fig. 5e and Supplementary Fig. 6a, e). Although both mC2 and hC2 CAR-T cells effectively controlled tumor growth, hC2 CAR-T cells, compared to mC2 CAR-T cells, showed a superior anti-tumor ability in U266 MM model evidenced by relatively lower human Ig $\lambda$  (tumor burden) (Fig. 5f) and better mouse survival (Fig. 5g). All mice treated with hC2 CAR-T cells displayed long-term survival and remained tumor free at the end of the experiment (week 12) (Fig. 5g). In MM.1S-A2 (Supplementary Fig. 6a–d) and KMS-12-BM-A2 (Supplementary Fig. 6e–h) mouse models, hC2 CAR-T cells also showed better anti-tumor activities evidenced by long-term survival rate up to 8 weeks post CAR-T cell infusion. Moreover, we evaluated the therapeutic efficacy of mC2 and hC2 CAR-T cells in PDAC mouse models (Fig. 5h

and Supplementary Fig. 6i). mC2 and hC2 CAR-T cells showed comparable anti-tumor activities in CFPAC-1 xenograft model (Fig. 5i–k). However, in the primary PDAC #1 PDX model, hC2 CAR-T cells showed a better anti-tumor activity compared to mC2 CAR-T cells, and all hC2 CAR-T cell-treated mice achieved long-term survival over 10 weeks (Supplementary Fig. 6j, k). Hence, while both mC2 and hC2 CAR-T cells exhibit comparable cytolytic ability in vitro, hC2 CAR-T cells show a better anti-tumor activity in vivo.

### hC2 CAR-T cells display central memory phenotype and exert better anti-tumor effects in vivo

Multiple mechanisms and clinical studies have shown that less differentiated memory T cells are required for a sustained CAR-T cell persistence in vivo<sup>41–43</sup>. To evaluate whether mC2 and hC2 CAR-T cells display distinct memory phenotypes, CAR-T cells generated from 4 healthy donors were analyzed for CCR7 and CD45RO expression by flow cytometry. hC2 CAR-T cells contained a higher percentage of cells (70%) that were CCR7<sup>+</sup> and CD45RO<sup>+</sup> (central memory phenotype), while mC2 CAR-T cells had a large population of CCR7<sup>−</sup> and CD45RO<sup>+</sup> effector memory cells compared to their counterpart (Fig. 6a, b). In co-culture with DKK1-A2 positive JeKo-1 tumor cells, hC2 CAR-T cells rapidly differentiated into effector memory phenotype to execute cytotoxic activity, while the memory phenotype of mC2 CAR-T cells had not significantly changed (Fig. 6c, d). mC2 and hC2 CAR-T cells were infused into JeKo-1 bearing mice for 7 days, and CCR7 expression on hC2 CAR-T cells was much higher than that of mC2 CAR-T cells, indicating hC2 CAR-T cells as less differentiated memory T cells in vivo (Supplementary Fig. 7a, b). Central memory-like hC2 CAR-T cells secreted lower amounts of IFN- $\gamma$  and TNF- $\alpha$  in both CD4 and CD8 positive subsets in response to JeKo-1, but Granzyme B secretion was similar to mC2 CAR-T cells (Fig. 6e–g). Notably, re-stimulation of the CAR-T cells by adding more tumor cells to the co-culture led to significantly higher IFN- $\gamma$ , TNF- $\alpha$ , and Granzyme B production by hC2 CAR-T cells compared to mC2 CAR-T cells (Fig. 6h–j). To further evaluate the long-term response of the CAR-T cells, we performed tumor rechallenge experiments. CAR-T cell-infused JeKo-1-bearing NSG mice were rechallenged with JeKo-1 tumor cells at 4 weeks post CAR-T cell infusion (Fig. 6k). In hC2 CAR-T cell-treated mice, tumor volumes were much lower, and more mice remained alive post tumor rechallenge (Fig. 6l, m). Improved hC2 CAR-T cell persistence was found in blood, lymph node, and spleen post tumor rechallenge (Fig. 6n). We also observed similar results in U266-rechallenge model that was controlled with naïve mice (Supplementary Fig. 7c–e). In CFPAC-1 rechallenge model, although all mice remained alive post-tumor rechallenge, tumor burdens in hC2 CAR-T cell-treated mice were significantly lower than those treated with mC2 CAR-T cells (Supplementary Fig. 7f–i). Together, these findings showed that hC2 CAR-T cells display a less-differentiated central memory phenotype

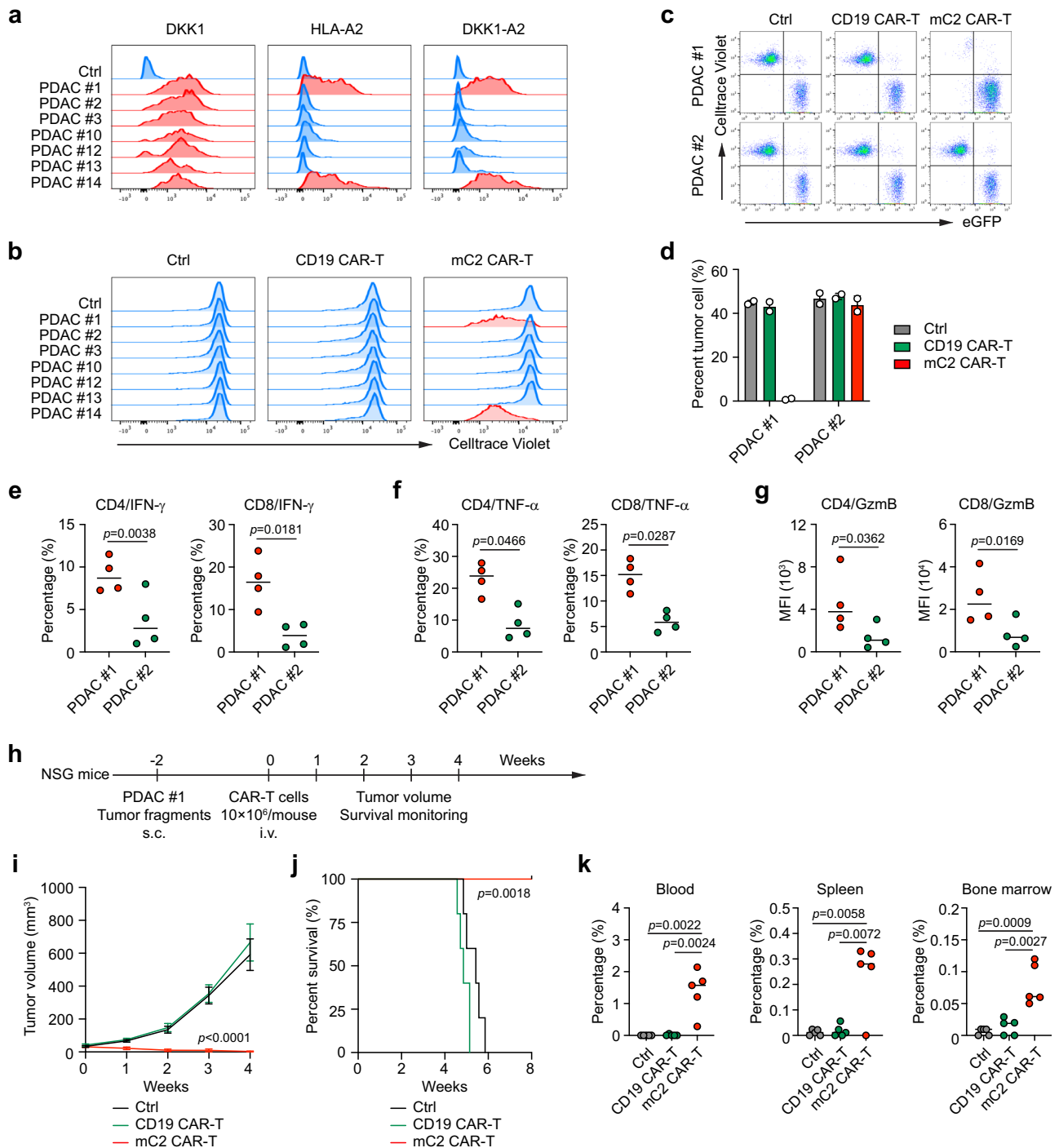


**Fig. 4 | In vivo anti-tumor effects of DKK1-A2 CAR-T cells in human PDAC PDX model.** **a** Expression of DKK1, HLA-A2, and DKK1-A2 complex by primary tumor cells of 7 randomly selected PDAC patients determined by flow cytometry. **b** CAR-T cell proliferation measured by dilution of Celltrace Violet, analyzed by flow cytometry. CAR-T cells were stained with Celltrace Violet and co-cultured with primary PDAC tumor cells from the patients at an E:T ratio of 1:1. **c** Representative flow staining, and **d** Summarized results depicting the in vitro cytolytic activity of CAR-T cells against primary PDAC cells determined by flow cytometry, measuring the number or percentage of primary tumor cells and CAR-T cells in their co-culture. Primary PDAC tumor cells were stained with Celltrace Violet and co-cultured with CAR-T cells for 72 h.  $n = 2$ , technical replicates. One-way ANOVA was used. **e-g** Percentages of IFN- $\gamma$ , TNF- $\alpha$ , and Granzyme B producing cells determined

by intracellular cytokine staining. CAR-T cells were co-cultured with primary PDAC tumor cells at an E:T ratio of 1:1 overnight.  $n = 4$ , biological replicates. Two-tailed Student's  $t$ -test was used. **h** Schema of PDAC PDX model treated with CAR-T cells, **i** Tumor volume of PDAC PDX mice measured weekly. Two-way ANOVA was used, **j** Survival of PDAC PDX mice monitored daily, Log-rank test was used, and **k** Percentages of CAR-T cells in blood, spleen, and bone marrow in PDAC PDX mice identified as GFP expression by flow cytometry before and post-CAR-T cell infusion. Percentage (%) was defined as the proportion of eGFP<sup>+</sup> CAR-T cells in blood cells, splenocytes, or bone marrow cells. Ctrl,  $n = 5$ ; CD19 CAR-T,  $n = 5$ ; mC2 CAR-T,  $n = 5$ ; biological replicates. Two-tailed Student's  $t$ -test was used. In some experiments, CD19 CAR-T cells were used as a control. Data shown as mean  $\pm$  SEM. Source data are provided as a Source data file.

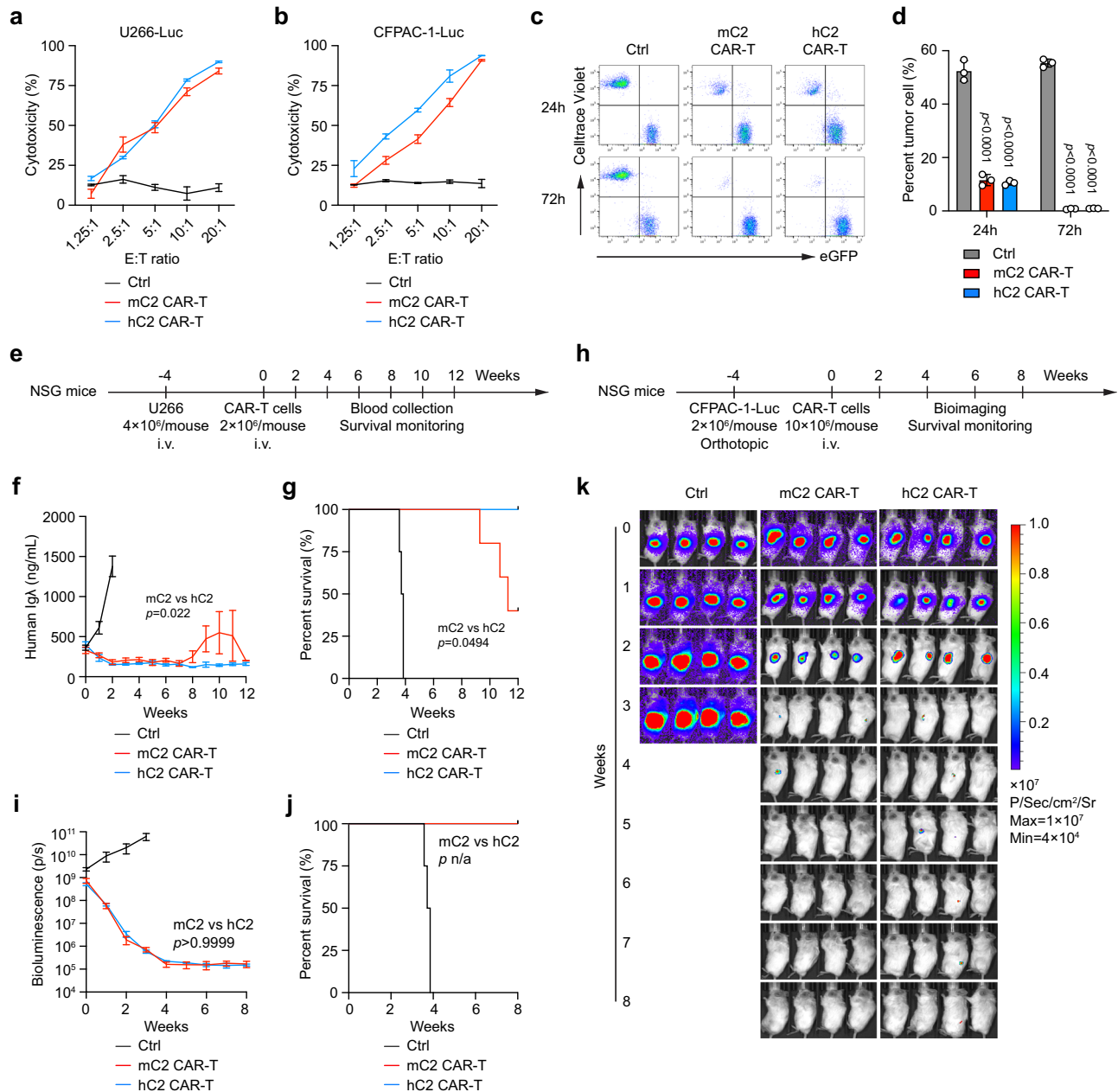


**Fig. 5 | Anti-tumor effects of DKK1-A2 CAR-T cells generated from a humanized C2 antibody.** **a, b** In vitro cytotoxicity of CAR-T cells determined by luciferase reporter assay. CAR-T cells were co-cultured with U266- or CFPAC-1-Luc tumor cells at indicated E:T ratios for 12 h.  $n = 2$ , technical replicates. **c** Representative flow staining, and **d** summarized results depicting the in vitro cytolytic activity of CAR-T cells against primary PDAC cells determined by flow cytometry, measuring the number or percentage of primary tumor cells and CAR-T cells in their co-culture. Primary PDAC tumor cells were stained with Celltrace Violet and co-cultured with CAR-T cells for 24 or 72 h.  $n = 3$ , technical replicates. One-way ANOVA was used. **e** Schema of U266 MM xenograft model treated with CAR-T cells, **f** Tumor burden measured as the level of human IgA secreted by U266 cells. Blood was collected

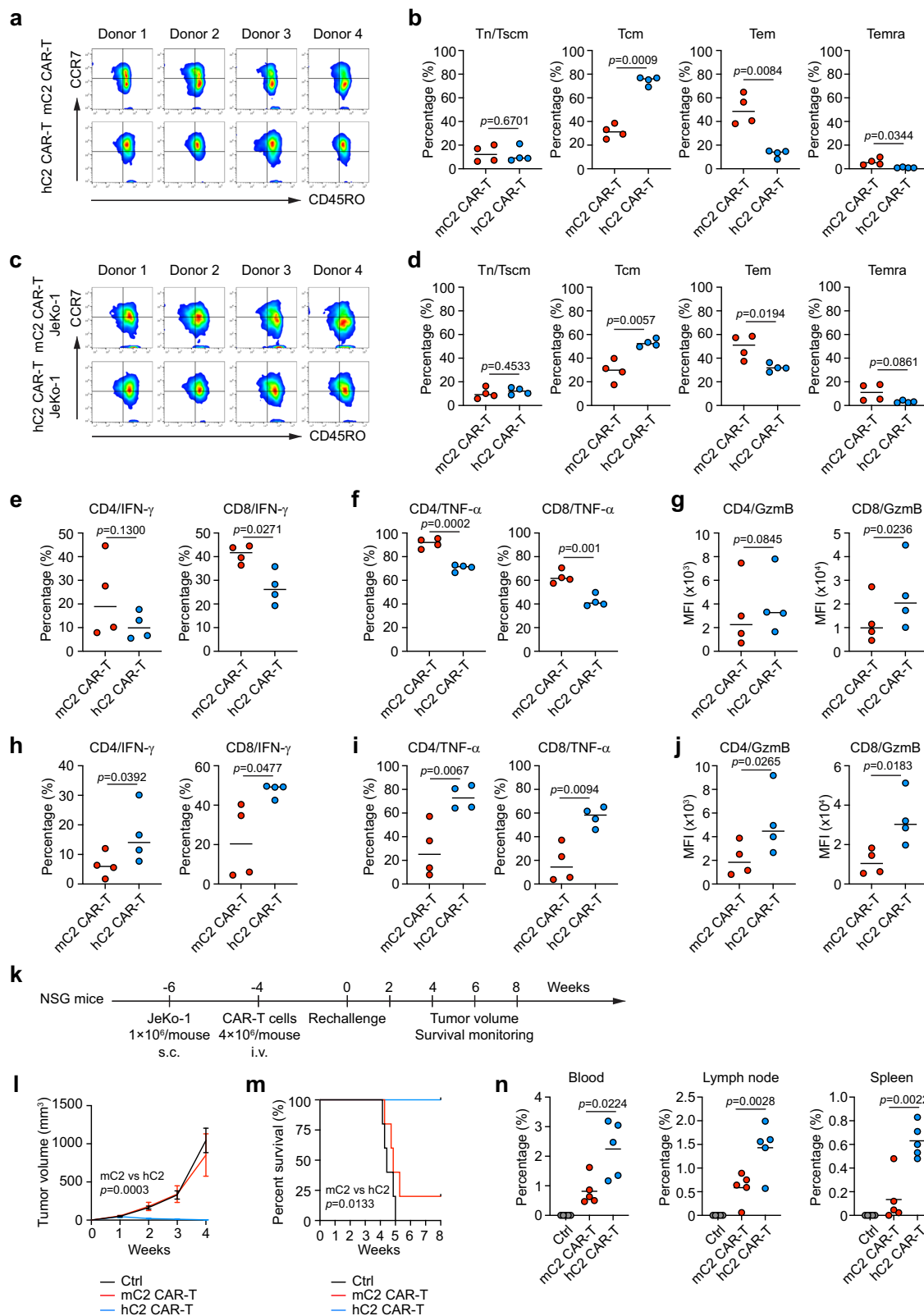
from U266 xenograft mice weekly, and serum was used for ELISA. Two-way ANOVA was used, and **g** Survival of U266 MM xenograft mice monitored daily before and post CAR-T cell infusion. Log-rank test was used. Ctrl,  $n = 4$ ; mC2 CAR-T,  $n = 5$ ; hC2 CAR-T,  $n = 5$ ; biological replicates. **h** Schema of CFPAC-1-Luc PDAC orthotopic xenograft model treated with CAR-T cells, **i** Tumor burden measured as bioluminescence intensity of CFPAC-1-Luc PDAC orthotopic xenograft mice, Two-way ANOVA was used, **j** Survival of CFPAC-1-Luc PDAC orthotopic xenograft mice monitored daily, Log-rank test was used, and **k** Bioluminescence images of CFPAC-1-Luc PDAC orthotopic xenograft mice before and post CAR-T cell infusion. Ctrl,  $n = 4$ ; mC2 CAR-T,  $n = 4$ ; hC2 CAR-T,  $n = 4$ ; biological replicates. Data shown as mean  $\pm$  SEM. Source data are provided as a Source data file.

that may have contributed to the long-term anti-tumor immunity against both MM and PDAC.

#### DKK1-A2 CAR-T cells do not cause damage to normal tissues

We assessed the expression of DKK1-A2 complex on human normal tissues with commercially available tissue arrays. Thirty-five different types of normal tissues from three HLA-A2 positive donors were stained with DKK1, HLA-A2, and DKK1-A2 (C2) antibodies. Although

some normal human tissues expressed DKK1 protein, all human normal tissues were stained negative for DKK1-A2 complex except the tonsil tissues (Fig. 7a and Supplementary Fig. 8a, b), indicating that the target for DKK1-A2 CAR-T cells is not present on most human tissues. To evaluate the potential hematological toxicity of DKK1-A2 CAR-T cells, peripheral blood mononuclear cell (PBMC) and bone marrow mononuclear cells (BMMC) from HLA-A2 positive donors were co-cultured with CAR-T cells and cell apoptosis was analyzed by flow



cytometry (Supplementary Fig. 8c). CD19 CAR-T cells effectively lysed B cells in both PBMC and BMBC, while mC2 or hc2 CAR-T cells did not cause significant cell death, evidenced by Annexin V and Caspase 3 staining in cell populations of PBMC or BMBC (Supplementary Fig. 8d–g). We then established a tripartite co-culture model<sup>44</sup> consisting of CAR-T cells, autologous monocytes and JeKo-1 cells for 24 h (Fig. 7b). In co-culture with hc2 CAR-T cells, significantly lower levels of

human IFN- $\gamma$  and IL-6 were observed in comparison to co-culture with mC2 CAR-T cells (Fig. 7c). To further assess the safety profile, we utilized a cytokine release syndrome model<sup>45</sup> by infusing a large dose ( $50 \times 10^6$  per mouse) of CAR-T cells intraperitoneally into JeKo-1 bearing mice (Fig. 7d). Similar to what was observed in vitro, CD19 and mC2 CAR-T cells expressed a comparable level of human IFN- $\gamma$  and mouse IL-6, while hc2 CAR-T cells had attenuated cytokine release

**Fig. 6 | hC2 CAR-T cells display central memory phenotype and exert better anti-tumor effects in vivo.** **a, b** mC2 or hC2 CAR-T cells were generated from 4 healthy donors. CCR7 and CD45RO expression on CAR-T cells was analyzed by flow cytometry, and **c, d** mC2 or hC2 CAR-T cells were generated from 4 healthy donors and then co-cultured with JeKo-1 tumor cells for 24 h. CCR7 and CD45RO expressions on CAR-T cells were analyzed by flow cytometry. Tn/Tscm: CCR7<sup>+</sup>CD45RO<sup>-</sup>, Tcm: CCR7<sup>+</sup>CD45RO<sup>+</sup>, Tem: CCR7<sup>-</sup>CD45RO<sup>+</sup>, and Temra: CCR7<sup>-</sup>CD45RO<sup>-</sup>. Percentage (%) was defined as the proportion of memory phenotypes relative to eGFP<sup>+</sup> CAR-T cells.  $n = 4$ , biological replicates. Two-tailed Student's *t*-test was used. **e–g** Percentages of IFN- $\gamma$ , TNF- $\alpha$  and Granzyme B producing CD4<sup>+</sup> or CD8<sup>+</sup> CAR-T cells analyzed by intracellular cytokine staining. mC2 and hC2 CAR-T cells were co-cultured with JeKo-1 tumor cells overnight.  $n = 4$ , biological replicates. Two-tailed Student's *t*-test was used. **h–j** Percentages of IFN- $\gamma$ , TNF- $\alpha$ , and Granzyme B

producing CD4<sup>+</sup> or CD8<sup>+</sup> CAR-T cells analyzed by intracellular cytokine staining. mC2 and hC2 CAR-T cells were co-cultured with JeKo-1 tumor cells overnight, followed by JeKo-1 tumor cells re-challenge overnight again.  $n = 4$ , biological replicates. Two-tailed Student's *t*-test was used. **k** Schema of JeKo-1-bearing NSG mice treated with mC2 or hC2 CAR-T cells, followed by JeKo-1 re-challenge controlled with naïve mice, **l** Tumor volume measured weekly post tumor cell re-challenge. Two-way ANOVA was used, **m** Survival of JeKo-1-bearing NSG mice. Log-rank test was used, and **n** Percentages of CAR-T cells in blood, lymph node, and spleen in JeKo-1-bearing NSG mice identified as GFP expression by flow cytometry at endpoint. Ctrl,  $n = 5$ ; mC2 CAR-T,  $n = 5$ ; hC2 CAR-T,  $n = 5$ ; biological replicates. Two-tailed Student's *t*-test was used. Data shown as mean  $\pm$  SEM. Source data are provided as a Source data file.

detected in peritoneal lavage fluid of treated mice (Fig. 7e). Body weight loss was also monitored as a readout. Both mC2 CAR-T cells and positive control CD19 CAR-T cells induced a more serious body weight loss compared to hC2 CAR-T cells (Fig. 7f).

Finally, we investigated the potential efficacy and toxicity of DKK1-A2 CAR-T cells in immunocompetent mice. We generated transgenic C57BL/6 mice expressing human DKK1 and HLA-A2 molecules (hDKK1-A2 mice) and developed murine CAR-T cells using mouse splenocytes targeting murine CD19 or human DKK1-A2 complex for in vivo tests. We first examined the potential hematological toxicity of the murine CAR-T cells. After intravenous infusion, murine CD19 CAR-T cells led to depletion of mouse B cells, while murine DKK1-A2 CAR-T cells did not affect cell populations in blood, spleen, or bone marrow (Fig. 7g–i). Moreover, we utilized the MM 5TGM1 and pancreatic cancer Pan02 syngeneic mouse models<sup>46,47</sup> by transducing murine 5TGM1 and Pan02 cells with human DKK1 and HLA-A2 molecules. After the tumor developed, mice were infused with CD19 or DKK1-A2 murine CAR-T cells. The results showed that DKK1-A2 but not CD19 CAR-T cells effectively controlled tumor growth in murine 5TGM1- and Pan02-bearing mice without obvious body weight change (Supplementary Fig. 9a–f). Since platelets were reported to express both DKK1 and MHC molecule<sup>48</sup>, we evaluated platelet cell count in hDKK1-A2 mice post CAR-T cell treatment. No significant change in platelet count was observed 7 days after CAR-T cell infusion, suggesting that DKK1-A2 CAR-T cells do not cause substantial depletion of circulating platelets (Supplementary Fig. 9g). Overall, these results clearly showed that DKK1-A2 CAR-T cells display a favorable safety profiles and may be less or non-toxic in human patients.

## Discussion

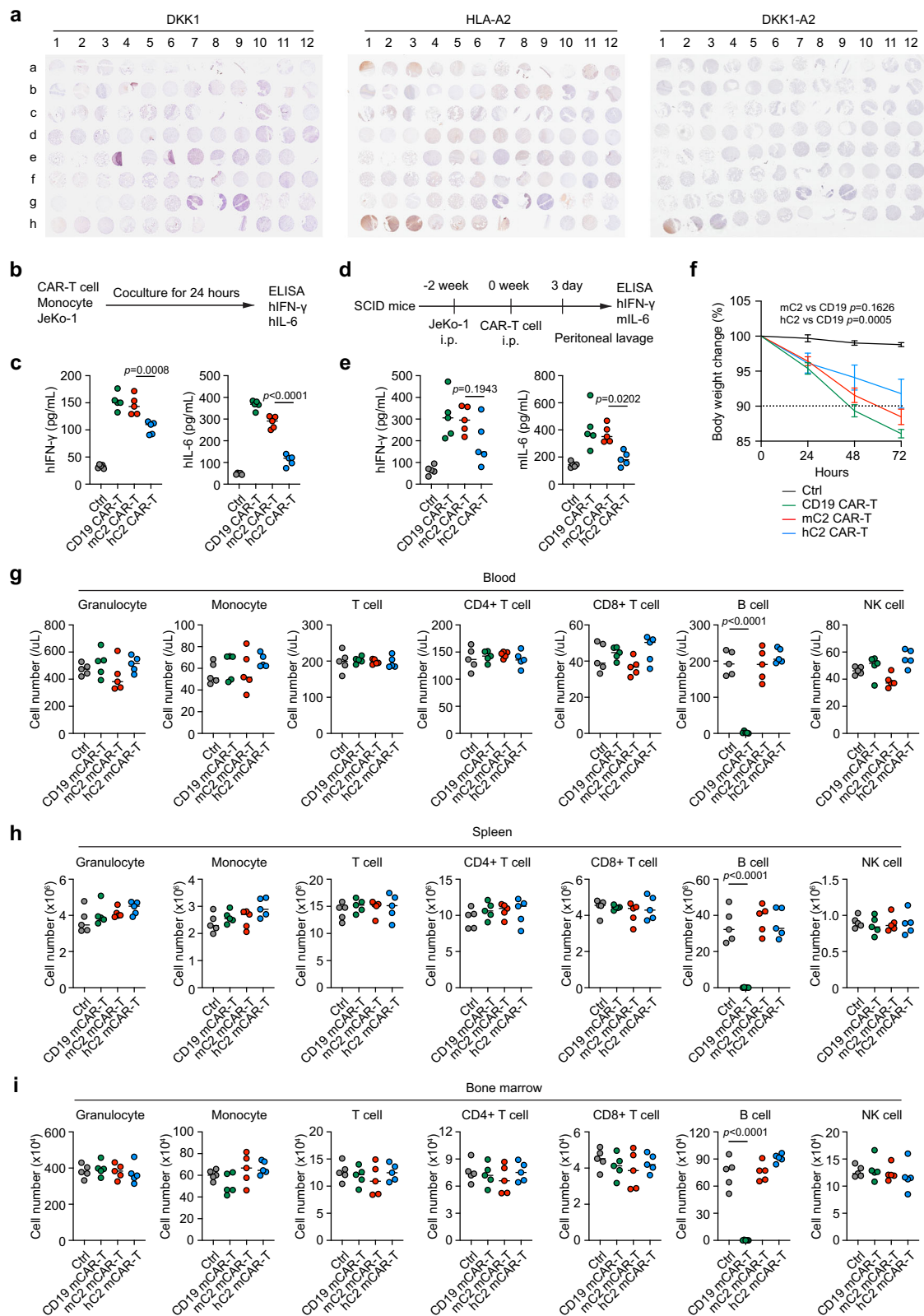
In this study, we investigated whether DKK1 is a clinically relevant target for cancer immunotherapy for both hematologic and solid tumors. We analyzed the gene datasets of MM, lymphoma and leukemia from Oncomine database, and found that MM patients expressed the highest level of *DKK1* among all types of hematologic tumors. We also analyzed gene datasets from GEPIA2 database for solid tumors and observed that most solid tumors highly expressed *DKK1* compared to normal tissues. These tumor types include pancreatic, lung, and esophagus cancer, and squamous head and neck cell carcinoma. Notably, although breast cancer expressed relatively lower levels of *DKK1* compare to the normal tissue, *DKK1* was highly expressed by TNBC, which is the most invasive type of breast cancer, accounting for 10–15% of all breast cancer cases<sup>49</sup>. Survival analysis from the GEPIA2 database showed that a higher expression of *DKK1* in patients had inferior overall and disease-free survivals in multiple solid tumors, indicating that DKK1 serves as a clinically relevant target for cancer immunotherapy.

Since DKK1 is a soluble protein participating in the Wnt/ $\beta$ -catenin signaling pathway, antibodies binding directly to DKK1 protein have a limited effect for cancer treatment<sup>50</sup>. We screened C2 antibody that recognizes DKK1-A2 complex on tumor cells and showed that C2

antibody displayed a high specific binding to DKK1-expressed HLA-A2 positive tumors including PDAC, NSCLC, and TNBC using IHC. The specificity of C2 antibody was confirmed by binding to multiple HLA-A2 positive tumor cell lines by flow cytometry. We also reported that C2 antibody had the ability to directly induce tumor cell apoptosis and lyse tumor cells by mediating antibody-dependent cellular cytotoxicity and complement-dependent cytotoxicity<sup>28</sup>. One limitation of C2 antibody is the restriction to HLA-A2, and the prevalence does not provide universal coverage to all patients. Exploring other DKK1-derived peptides presented by additional HLA alleles would be an important future direction. Such studies could expand to a broader patient population and enhance the translational potential.

Based on the specificity and efficacy of C2 antibody, we translated C2 antibody into CAR-T cell immunotherapy for both hematologic and solid tumors. DKK1-A2 CAR-T cells showed strong anti-tumor activity against multiple tumor cell lines in vitro and in human xenograft models of MM and solid tumors, as well as in primary PDAC patient-derived tumor models. In vitro tumor cytolytic activity was confirmed by a luciferase-based cytotoxicity assay, proliferation and cytokine release by the CAR-T cells, and in vivo anti-tumor activity against MM and solid tumors was demonstrated by subcutaneous, orthotopic, and metastatic xenograft models. To recapitulate the histology and genetic profile of human PDAC tumors, primary PDAC cells and PDX model were established and the efficacy of DKK1-A2 CAR-T cells was confirmed. There are limitations about these tumor models. In the CFPAC-1 PDAC orthotopic models, CD19 CAR-T cell control was not included mainly because of the difficulty in establishing the tumor model and limited number of mice. In addition, NSG mice are deficient in a fully functional immune system, which neglects the impact of the host immune system on CAR-T cell response. To validate the results in more physiologically relevant models, we performed CAR-T cell treatment in murine syngeneic models using 5TGM1 and Pan02 tumor cell lines. Another limitation is that only one primary PDAC patient sample underwent three passages and was used for in vivo efficacy testing, mainly due to difficulties and the long time to establish stable PDX models.

CAR-T cell therapies are being widely developed and have proven to be efficacious in clinical studies<sup>51</sup>. Hematologic tumors typically involve uniform and well-characterized antigen targets, such as BCMA for MM<sup>52</sup>, CD19 for B-cell leukemia and lymphoma<sup>53</sup>, and CD30 for Hodgkin lymphoma and some T-cell lymphomas<sup>54</sup>. Solid tumors present more challenges due to antigen heterogeneity and expression on normal tissues, such as HER2 for breast cancer and glioma<sup>55,56</sup>, claudin 18.2 for gastric cancer<sup>11,57</sup>, and GPC3 for hepatocellular cancer<sup>58</sup>. Since limited overlapping antigens are expressed on hematologic and solid tumor cells, CAR-T cells targeting both hematologic and solid tumors have been rarely studied or developed. Dual-targeting CAR-T cells offer significant potential for across multiple cancer therapies, but the complexity in design and manufacturing, as well as high risk of off-target effects, are still huge obstacles to be solved<sup>59,60</sup>. To our knowledge, our studies offer a potential well-defined DKK1-A2 target across



multiple tumors, including MM, pancreatic, lung, and breast cancer for CAR-T cell therapies.

Besides the original C2 antibody generated from mice, we also engineered a humanized C2 antibody with the human constant regions. CAR-T cells generated from the scFv of hC2 antibody showed similar cytolytic activity with mC2 CAR-T cells against MM and PDAC cell lines in vitro but exhibited superior anti-tumor ability in vivo.

These surprising results sparked our curiosity to explore the underlying mechanisms. Our results showed that hC2 CAR-T cells displayed a CCR7<sup>+</sup> and CD45RO<sup>+</sup> central memory-like phenotype and responded more intensely than mC2 CAR-T cells to tumor cell rechallenge in vitro<sup>61,62</sup>. Notably, this memory phenotype of hC2 CAR-T cells contributed to long-term tumor control, evidenced by the protective effect post-tumor rechallenge in vivo. Increasing evidence suggests

**Fig. 7 | Tissue toxicity studies of DKK1-A2 CAR-T cells.** **a** Immunohistochemistry staining of human normal tissue microarray containing 35 different types of normal tissues (including Marker) from three HLA-A2 positive donors stained with DKK1, HLA-A2 and DKK1-A2 complex. **b, c** Levels of secreted human IFN- $\gamma$  and IL-6 in co-culture of CAR-T cells with autologous monocytes and JeKo-1 tumor cells for 24 h determined by ELISA.  $n = 5$ , technical replicates. One-way ANOVA was used. **d, e** Levels of secreted human IFN- $\gamma$  and murine IL-6 in the peritoneal lavage fluid of JeKo-1 bearing mice treated with intraperitoneally infused an excessive dose of

CAR-T cells determined 3 days post CAR-T cell infusion.  $n = 5$ , biological replicates. One-way ANOVA was used. **f** Body weight change of SCID mice transferred with the excessive dose of CAR-T cells monitored every 24 h.  $n = 5$ , biological replicates. Two-way ANOVA was used. **g–i** Numbers of immune cell populations in blood, spleen and bone marrow of hDKK1-A2 mice treated with murine DKK1-CAR-T cells analyzed by flow cytometry.  $n = 5$ , biological replicates. One-way ANOVA was used. In most experiments, CD19 CAR-T cells were used as a control. Data shown as mean  $\pm$  SEM. Source data are provided as a Source data file.

that the affinity of the antibody may play a significant role in regulating the anti-tumor activity of CAR-T cells. Ghorashian and coworkers generated a CD19 CAR with a lower affinity than FMC63, and showed increased proliferation and cytotoxicity *in vitro*, as well as enhanced anti-tumor activity compared with FMC63 CAR-T cells<sup>63</sup>. Shabaneh and co-workers also showed that low-affinity HER2 CAR-T cells mediated an enhanced anti-tumor immunity and attenuated on-target off-tumor toxicity<sup>64</sup>. Multiple explanations demonstrated that low-affinity of CAR molecules provided physiological receptor signaling and prevented exhaustion and induction of early memory phenotype<sup>65</sup>. Based on our data of C2 antibody characteristics, the binding affinity of hC2 antibody to DKK1-A2 complex (KD = 19 nM) was lower than that of mC2 antibody (KD = 1.82 nM), which may provide a reasonable explanation of the difference between mC2 and hC2 CAR-T cells.

Although our studies demonstrated the anti-tumor efficacy of DKK1-A2 CAR-T cells in various tumor models, the on- and off-target toxicities against normal tissues remain a concern. Immunohistochemistry staining of normal tissue arrays demonstrated the absent expression of DKK1-A2 complex on almost all human normal tissues but tonsil tissues. The possible reason for DKK1-A2 complex expression on tonsil could be tonsil-related inflammation, as DKK1 serves as an immunomodulator in tissue inflammation and could be upregulated under these conditions<sup>66</sup>. Flow cytometry analysis also showed that DKK1-A2 CAR-T cells did not display detectable toxicities towards cellular subsets of blood and bone marrow *in vitro*. In addition, DKK1-A2 CAR-T cells did not induce significant killing of blood, spleen, and bone marrow cells *in vivo*. Together, these results demonstrated a favorable safety profile of DKK1-A2 CAR-T cells. However, the current off-target screening strategy was limited in scope, as broader panels of HLA-A2<sup>+</sup> primary human cells or iPSC-derived tissues were not evaluated. Incorporating such models in future studies will be important to assess potential off-target toxicities more comprehensively and to further support the translational potential of DKK1-A2 CAR-T cells.

Since hC2 CAR-T cells presented a central memory phenotype, we speculated that this phenotype would contribute to mitigating cytokine release syndrome. Data from an *in vitro* tripartite co-culture experiment<sup>44</sup> and a cytokine release syndrome mouse model<sup>45</sup> were performed to test our hypothesis. Arcangeli's data illustrated that naive/stem memory-like CAR-T cell manufacturing showed an enhanced anti-tumor immunity while curtailing cytokine release syndromes<sup>44</sup>. Similarly, our studies demonstrated that hC2 CAR-T cells exhibited a central memory-like phenotype and conferred an enhanced anti-tumor activity with long-term immunological protection.

Overall, we developed DKK1-A2 CAR-T cells for the treatment of human hematologic and solid tumors. DKK1-A2 CAR-T cells exhibit a favorable safety profile without detectable on- or off-target toxicities against normal tissues. Thus, our results suggest the applicability of DKK1-A2 CAR-T cells in the treatment of human cancer.

## Methods

### Ethical statement

Our research complies with all relevant ethical regulations. The use of primary tumor tissues was approved by the Institutional Review Board at the Houston Methodist Research Institute. All animal studies were

approved by the Institutional Animal Care and Use Committee of the Houston Methodist Research Institute.

### Human and mouse cell lines

Human mantle cell lymphoma cell line JeKo-1, Burkitt's lymphoma cell line Daudi, MM cell lines U266, KMS-26, ARP-1, KMS-11, KMS-12-BM, and MM.1S, PDAC cell lines CFPAC-1, PANC-1, MIA PaCa-2, and PL45, NSCLC cell lines NCI-H441 and NCI-H266, and TNBC cell lines MDA-MB-231 and MDA-MB-468 were purchased from American Type Culture Collection or obtained from Arkansas Cancer Research Center. KMS-12-BM-A2, KMS.1S-A2, and PL45-A2 were generated by transducing with the human gene HLA-A\*0201. JeKo-1-KO was generated by CRISPR/Cas9 gene-editing technology. Firefly Luciferase stably transduced-JeKo-1, Daudi, U266, KMS-26, CFPAC-1, PANC-1, NCI-H441, MDA-MB-231, KMS-12-BM-A2, KMS.1S-A2, and PL45-A2 were generated by transducing with luciferase gene. Murine MM 5TGM1-DKK1-A2 and Pan02-DKK1-A2 cells were generated by transducing the cells with human HLA-A2 and DKK1 genes. All cell lines were cultured in complete RPMI 1640 medium or Dulbecco modified Eagle's medium supplemented with 10% FBS and 1% penicillin and streptomycin.

### Animals

NSG and SCID mice were purchased from the Jackson Laboratory. hDKK1-A2 mice were generated by crossing HLA-A2 transgenic mice with DKK1 transgenic mice by Cyagen Biosciences. Male and female 6–8-week-old mice were used in the studies. Mice were maintained in American Association of Laboratory Animal Care-accredited facilities, and all studies were approved by the Institutional Animal Care and Use Committee of Houston Methodist Research Institute. We have complied with all relevant ethical regulations. For MM mouse models, the maximal tumor burden permitted by our ethics committee is the point when they develop signs of hind limb paralysis. For solid tumor mouse models, the maximal tumor burden permitted by our ethics committee is no more than 20 mm in diameter. In our study, the maximal tumor burden was not exceeded.

### Human samples

Human whole peripheral blood was purchased from the Gulf Coast Regional Blood Center, Houston, Texas. Human PDAC, NSCLC, and TNBC tissues were obtained from surgical resections of patients at Houston Methodist Hospital. Human tumor tissues were used for establishment of primary patient-derived tumor cells and xenograft model, as well as immunohistochemistry and tissue microarray studies. Utility of human samples in this study was approved by the institutional review board at the Houston Methodist Research Institute.

### Plasmid construction and retrovirus preparation

Plasmid construction and retrovirus preparation were described previously<sup>67</sup>. Gene sequence of light and heavy chain of murine or humanized C2 antibody were obtained from cDNA of C2 hybridomas amplified by using PCR. mC2, hC2, or FMC63 scFv-based chimeric antigen receptor were cloned into SFG retroviral vector, followed by CD8 $\alpha$  hinge and transmembrane, 4-1BB intracellular costimulatory domain, CD3 $\zeta$  intracellular signaling domain and eGFP. 293T cells were

seeded in 100 mm cell culture dish and transfected with a plasmid mixture of chimeric antigen receptor retroviral vector, packaging plasmid encoding Gag/Pol, and envelope plasmid encoding RD114 by using Lipofectamine 3000 transfection reagent. Culture supernatant was collected 48 and 72 h after transduction, and retrovirus was precipitated by PEG-400.

### Retrovirus transduction and CAR-T cell culture

Transduction of T cells was described previously<sup>68,69</sup>. Peripheral blood mononuclear cells were obtained by Ficoll density gradient centrifugation. CD3<sup>+</sup> T cells were isolated by immunomagnetic negative selection kit from STEMCELL Technologies. T cells were activated with CD3/CD28 Dynabeads or 10 µg/mL anti-CD3/CD28 antibodies for 24 h and transduced with retrovirus on RetroNectin-coated plates. Three days later, T cells were expanded in complete RPMI 1640 medium supplemented with human IL-2. Two weeks after transduction, T cells were collected for in vitro or in vivo experiments. Transduction efficiency was determined by the percentage of eGFP expression analyzed by flow cytometry.

### Flow cytometry

Tumor cell lines were harvested and resuspended in FACS buffer (PBS with 1% FBS and 1 mM EDTA). First, tumor cells were stained with FcR blocker and surface-stained with BUV395-conjugated HLA-A2 antibody (BD Bioscience, 1 µg/mL) and Alexa Fluor 647-conjugated mC2 antibody (1 µg/mL). After wash with FACS buffer, tumor cells were fixed and permeabilized by using BD Cytofix/Cytoperm Fixation/Permeabilization Kit. Tumor cells were intracellularly stained with DKK1 antibody (Santa Cruz Biotechnology, 1 µg/mL), and then Alexa Fluor 488-conjugated goat anti-mouse IgG1 antibody (Life Technologies, 1 µg/mL). For the PDX model, tumor tissues were digested with Collagenase and DNase I. Tumor cells were harvested and stained with purified CEA antibody (NeoBiotechnologies, 1 µg/mL), followed by staining with Alexa Fluor 594-conjugated goat anti-mouse IgG antibody (Life Technologies, 1 µg/mL), along with anti-DKK1, HLA-A2, or mC2 antibodies as described above. All fluorescent antibodies were controlled by corresponding isotype control (1 µg/mL). After wash with permeabilization buffer, tumor cells were resuspended in FACS buffer and analyzed by flow cytometry.

### Cytotoxicity assay

Luciferase reporter assay was used to evaluate the cytotoxicity of CAR-T cells. Firefly luciferase stably transduced tumor cells were seeded onto a 96-well plate overnight at 0.05 million per well. The next day, serial dilutions of CAR-T cells were prepared according to the effector to target (E:T) ratio and incubated with target cells for the indicated time. The supernatant was gently discarded, D-luciferin was added to each well for 5-min incubation, and data was measured by a microplate reader. The cytotoxicity of CAR-T cells was quantified by converting the obtained values to percentage of specific lysis by the following equation:  $[1 - (S-E)/(T-B)] * 100\%$ , where S is the value of luminescence of the sample well, E is the value of luminescence of the effector cell well, T is the mean value of luminescence of target cell well, and B is the mean value of luminescence of blank well. Flow cytometry-based cytotoxicity assay was also used to evaluate lysis ability of CAR-T cells<sup>70</sup>. Briefly, target cells were stained with Celltrace Violet and co-cultured with effector cells at an E:T ratio of 1:1 for 24–72 h. After that, percentages of tumor cells and CAR-T cells were analyzed by flow cytometry.

### Proliferation assay

CAR-T cells were stained with Celltrace Violet at the concentration of 1 µM and then co-cultured with tumor cells at a E:T ratio of 1:1 for 72 h. Proliferation of CAR-T cells was determined by dilution of Celltrace

Violet in CAR-T cells. Data were obtained with flow cytometry and analyzed by FlowJo software.

### Cytokine assay

Cytokine secretion analysis was performed using flow cytometry-based techniques<sup>71</sup>. Briefly, CAR-T cells were incubated with target tumor cells in 96-well plates overnight in the presence of phorbol myristate acetate, ionomycin, and brefeldin A. After that, cells were harvested then stained with FcR blocker and fluorescent antibodies specific to CD3, CD4, and CD8 on ice. After fixation and permeabilization, cells were intracellularly stained with fluorescent antibodies specific to IFN-γ, TNF-α, or Granzyme B. Data were acquired with flow cytometry and analyzed with FlowJo software. Cytokine secretion was also analyzed by ELISA according to the manufacturer's instructions.

### Human xenograft mouse models

Luciferase stably transduced human myeloma U266, KMS-26, KMS-12-BM, and MM.1S, pancreatic cancer CFPAC-1 and PANC-1, lung cancer NCI-H441, and breast cancer MDA-MB-231 xenograft models were used to evaluate the therapeutic efficacy of CAR-T cells in vivo. For MM models, tumor cells were inoculated intravenously into NSG mice. For subcutaneous solid tumor models, tumor cells were inoculated subcutaneously into NSG mice. For metastatic tumor models, tumor cells were inoculated intravenously into NSG mice. For orthotopic PDAC or breast tumor models, tumor cells were implanted into the pancreas or mammary pad of NSG mice, respectively. Control, CD19, mC2, or hC2 CAR-T cells were intravenously transferred into tumor-bearing mice. For the JeKo-1 rechallenge experiment, JeKo-1 tumor cells were inoculated subcutaneously into the contralateral side of the mouse back relative to the primary tumor. For the U266 rechallenge experiment, U266 tumor cells were inoculated intravenously into the mice. For the CFPAC-1-Luc rechallenge experiment, CFPAC-1-Luc tumor cells were inoculated subcutaneously into the contralateral side of the mouse back relative to the primary tumor. The numbers of rechallenge tumor cells were the same as the primary tumor inoculation. Tumor burdens were evaluated weekly by bioluminescence on IVIS imaging system and images were processed by Living Image software<sup>72</sup>. For MM models, serum levels of human Igλ secreted by MM cells were determined by ELISA<sup>73</sup>. Survival and body weight of tumor bearing mice were monitored. Tumor volume was calculated by the formula: tumor volume =  $0.5 * length * width^2$ . Mice were sacrificed when undergoing cancer cachexia, or tumor diameter exceeded more than 20 mm, or tumor volume exceeded more than 2000 mm<sup>3</sup>. Mice were sacrificed at the indicated time point for ex vivo analysis.

### Patient-derived tumor cells and xenograft model

Human PDAC tumor tissues were obtained from surgical resections of PDAC patients at Houston Methodist Hospital. Necrotic tissue and non-tumor tissue were removed under sterile conditions, and tumor tissues were cut into small pieces (2–4 mm<sup>3</sup>). Primary PDAC tumors were expanded in the flanks of NSG mice for 1–3 passages, allowing for greater expansion of tumor tissues<sup>40</sup>. For primary patient-derived tumor cells, tumor fragments from xenograft mice models were digested by DNase I and collagenase IV. Single tumor cell suspension was filtered for cytotoxicity, proliferation, and cytokine assay in vitro as described previously<sup>74</sup>. Tumor fragments were implanted into subcutaneous space of 6–8 weeks NSG mice. Fourteen days post-tumor implantation, mice were treated with CAR-T cells intravenously. Tumor volume and body weight were monitored weekly, and survival was monitored daily. Tumor volume was calculated by the formula: tumor volume =  $0.5 * length * width^2$ . Mice were sacrificed when undergoing cancer cachexia, tumor diameter exceeded more than 20 mm, or tumor volume exceeded more than 2000 mm<sup>3</sup>. Mice were sacrificed at the indicated time point for ex vivo analysis.

## Immunohistochemistry, immunofluorescence, and tissue microarray

Human PDAC, NSCLC, and TNBC tumor and normal tissues were obtained from Houston Methodist Hospital. Immunohistochemistry was described before<sup>75</sup>. Formalin-fixed, paraffin-embedded tissue sections (4–5 μm) were deparaffinized in xylene and rehydrated through graded ethanol. Slides were treated with a heat-induced epitope retrieval solution for 10–20 min. Endogenous peroxidase activity was blocked with 3% hydrogen peroxide, followed by incubation with a blocking solution to prevent non-specific binding. Sections were incubated with the primary antibody of DKK1 (Santa Cruz Biotechnology, 10 μg/mL), HLA-A2 (Santa Cruz Biotechnology, 10 μg/mL), DKK1-A2 (mC2/hC2, 10 μg/mL), or CEA (NeoBiotechnologies, 10 μg/mL) overnight at 4 °C. All samples were controlled with corresponding isotype control at the same concentrations. A secondary antibody conjugated to horseradish peroxidase was applied, and the signal was visualized using diaminobenzidine as the chromogen. Slides were analyzed under a microscope. Immunofluorescence was described before<sup>76</sup>. Mouse tumor tissues were collected, embedded into OCT compound, and rapidly frozen in dry ice. The frozen blocks were then mounted on a cryostat and sectioned. Sections were collected on glass slides, fixed, and then stained with the TUNEL assay kit (Thermo Fisher) and DAPI. Slides were analyzed under a microscope. Tissue microarray was purchased from Tissue Array company. Slides were stained with an antibody against DKK1, HLA-A2, and DKK1-A2 as described above and analyzed under a microscope. Quantitative data of the DKK1-A2 complex of tissue microarray were analyzed and obtained by ImageJ software.

## Cytokine release syndrome model

For the cytokine release syndrome model in vitro, a tripartite coculture of CAR-T cells, autologous monocytes, and JeKo-1 tumor cells were performed for 24 h at a ratio of 1:1:1<sup>44</sup>. Supernatants were collected, and human IFN-γ and IL-6 were measured by ELISA. For cytokine release syndrome model in vivo<sup>45</sup>, SCID mice were inoculated with JeKo-1 tumor cells intraperitoneally for 2 weeks followed by a large dose (50 × 10<sup>6</sup> per mouse) of CAR-T cells infusion intraperitoneally. Peritoneal lavage was collected 3 days post CAR-T cells infusion, and human IFN-γ and murine IL-6 were measured by ELISA.

## Hematologic toxicity assay

For in vitro hematologic toxicity assay, CAR-T cells were co-cultured with PBMC or BMMC for 4 h at a ratio of 1:1. Cultured cells were stained with anti-human CD11b, CD11c, CD3, CD4, CD8, CD19, NK1.1, CD34, and CD71 antibodies. Cell apoptosis was determined by staining the cells with anti-human Annexin V or Caspase 3 antibodies and analyzed by flow cytometry. For in vivo hematologic toxicity assay, hDKK1-A2 mice were infused with murine CAR-T cells intravenously. Blood, spleen, and bone marrow were collected on 7 days post CAR-T cell infusion. Single cell suspension was prepared and stained with anti-mouse CD11b, CD11c, CD3, CD4, CD8, CD19, and NK1.1 antibodies. Cell counts were normalized by counting beads and analyzed by flow cytometry. For the platelet cell count experiment, hDKK1-A2 mice were transferred with control, CD19, mC2, or hC2 CAR-T cells. One week after CAR-T cell transfer, whole blood was collected, and platelets were stained with CD41 and CD61 antibodies. Platelet cell count was analyzed by flow cytometry.

## Statistical analysis

All graphs and statistical analysis were generated by GraphPad Prism software. Student's *t* test or ANOVA analysis was performed for statistical analysis. Log-rank test was performed for survival analysis. Simple linear regression was performed for correlation analysis. A *p* value < 0.05 was considered statistically significant. Results are presented as mean ± SEM unless otherwise indicated.

## Reporting summary

Further information on research design is available in the Nature Portfolio Reporting Summary linked to this article.

## Data availability

This paper does not report any sequencing or proteomics data. Other previous published patient datasets used in the study can get access with the following accession numbers: GSE13591, GSE2350, GSE13159, GSE16515, GSE10072, EGAS00000000083 and GEPIA2. All the other data supporting the findings of this study are available with in the article, supplementary information and source files. Source data are provided with this paper.

## References

- San-Miguel, J. et al. Cilta-cel or standard care in lenalidomide-refractory multiple myeloma. *N. Engl. J. Med.* **389**, 335–347 (2023).
- Maude, S. L. et al. Tisagenlecleucel in children and young adults with B-cell lymphoblastic leukemia. *N. Engl. J. Med.* **378**, 439–448 (2018).
- Schuster, S. J. et al. Tisagenlecleucel in adult relapsed or refractory diffuse large B-cell lymphoma. *N. Engl. J. Med.* **380**, 45–56 (2019).
- Locke, F. L. et al. Axicabtagene ciloleucel as second-line therapy for large B-cell lymphoma. *N. Engl. J. Med.* **386**, 640–654 (2022).
- Neelapu, S. S. et al. Axicabtagene ciloleucel as first-line therapy in high-risk large B-cell lymphoma: the phase 2 ZUMA-12 trial. *Nat. Med.* **28**, 735–742 (2022).
- Rodriguez-Otero, P. et al. Ide-cel or standard regimens in relapsed and refractory multiple myeloma. *N. Engl. J. Med.* **388**, 1002–1014 (2023).
- Brudno, J. N., Maus, M. V. & Hinrichs, C. S. CAR T cells and T-Cell therapies for cancer: a translational science review. *JAMA* **332**, 1924–1935 (2024).
- Albelda, S. M. CAR T cell therapy for patients with solid tumours: key lessons to learn and unlearn. *Nat. Rev. Clin. Oncol.* **21**, 47–66 (2024).
- Erler, P. et al. Multi-armed allogeneic MUC1 CAR T cells enhance efficacy and safety in triple-negative breast cancer. *Sci. Adv.* **10**, eadn9857 (2024).
- Batra, S. A. et al. Glypican-3-specific CAR T cells coexpressing IL15 and IL21 have Superior Expansion and Antitumor Activity against Hepatocellular Carcinoma. *Cancer Immunol. Res.* **8**, 309–320 (2020).
- Qi, C. et al. Claudin18.2-specific CAR T cells in gastrointestinal cancers: phase 1 trial interim results. *Nat. Med.* **28**, 1189–1198 (2022).
- Sterner, R. C. & Sterner, R. M. CAR-T cell therapy: current limitations and potential strategies. *Blood Cancer J.* **11**, 1–11 (2021).
- Niida, A. et al. DKK1, a negative regulator of Wnt signaling, is a target of the β-catenin/TCF pathway. *Oncogene* **23**, 8520–8526 (2004).
- Yamamoto, H., Sakane, H., Yamamoto, H., Michiue, T. & Kikuchi, A. Wnt3a and Dkk1 regulate distinct internalization pathways of LRP6 to tune the activation of β-Catenin Signaling. *Dev. Cell* **15**, 37–48 (2008).
- Yamamoto, H., Komekado, H. & Kikuchi, A. Caveolin is necessary for Wnt-3a-dependent internalization of LRP6 and accumulation of β-catenin. *Dev. Cell* **11**, 213–223 (2006).
- Yi, Q. et al. DKK-1 is a widely expressed, potent tumor-associated antigen in multiple myeloma recognized by cytotoxic T lymphocytes. *Blood* **106**, 3467 (2005).
- Igbinigie, E., Guo, F., Jiang, S.-W., Kelley, C. & Li, J. Dkk1 involvement and its potential as a biomarker in pancreatic ductal adenocarcinoma. *Clin. Chim. Acta Int. J. Clin. Chem.* **488**, 226–234 (2019).
- Yamabuki, T. et al. Dikkopf-1 as a novel serologic and prognostic biomarker for lung and esophageal carcinomas. *Cancer Res.* **67**, 2517–2525 (2007).

19. Voorzanger-Rousselot, N. et al. Increased Dickkopf-1 expression in breast cancer bone metastases. *Br. J. Cancer* **97**, 964–970 (2007).
20. Niu, J. et al. EGF promotes DKK1 transcription in hepatocellular carcinoma by enhancing the phosphorylation and acetylation of histone H3. *Sci. Signal.* **13**, eabb5727 (2020).
21. Pinzone, J. J. et al. The role of Dickkopf-1 in bone development, homeostasis, and disease. *Blood* **113**, 517–525 (2009).
22. Shi, T. & Wei, J. Targeting DKK1 to remodel the tumor micro-environment and enhance immune checkpoint blockade therapy. *J. Clin. Oncol.* **43**, 350–353 (2025).
23. D’Amico, L. et al. Dickkopf-related protein 1 (Dkk1) regulates the accumulation and function of myeloid derived suppressor cells in cancer. *J. Exp. Med.* **213**, 827–840 (2016).
24. Qian, J. & Yi, Q. DKK1 as a novel target for myeloma immunotherapy. *Oncol Immunology* **1**, 756–758 (2012).
25. Qian, J. et al. Dickkopf-1 (DKK1) is a widely expressed and potent tumor-associated antigen in multiple myeloma. *Blood* **110**, 1587–1594 (2007).
26. Yi, Q. Novel immunotherapies. *Cancer J.* **15**, 502 (2009).
27. Olivier, T., Haslam, A., Tuia, J. & Prasad, V. Eligibility for human leukocyte antigen-based therapeutics by race and ethnicity. *JAMA Netw. Open* **6**, e2338612 (2023).
28. Qian, J. et al. Development of therapeutic monoclonal antibodies against DKK1 peptide-HLA-A2 complex to treat human cancers. *J. Immunother. cancer* **12**, e008145 (2024).
29. Agnelli, L. et al. A SNP microarray and FISH-based procedure to detect allelic imbalances in multiple myeloma: an integrated genomics approach reveals a wide gene dosage effect. *Genes Chromosomes Cancer* **48**, 603–614 (2009).
30. Basso, K. et al. Reverse engineering of regulatory networks in human B cells. *Nat. Genet.* **37**, 382–390 (2005).
31. Haferlach, T. et al. Clinical utility of microarray-based gene expression profiling in the diagnosis and subclassification of leukemia: report from the International Microarray Innovations in Leukemia Study Group. *J. Clin. Oncol. Off. J. Am. Soc. Clin. Oncol.* **28**, 2529–2537 (2010).
32. Tang, Z., Kang, B., Li, C., Chen, T. & Zhang, Z. GEPIA2: an enhanced web server for large-scale expression profiling and interactive analysis. *Nucleic Acids Res.* **47**, W556–W560 (2019).
33. Kleeff, J. et al. Pancreatic cancer. *Nat. Rev. Dis. Prim.* **2**, 1–22 (2016).
34. Pei, H. et al. FKBP51 affects cancer cell response to chemotherapy by negatively regulating Akt. *Cancer Cell* **16**, 259–266 (2009).
35. Landi, M. T. et al. Gene expression signature of cigarette smoking and its role in lung adenocarcinoma development and survival. *PLoS ONE* **3**, e1651 (2008).
36. Curtis, C. et al. The genomic and transcriptomic architecture of 2000 breast tumours reveals novel subgroups. *Nature* **486**, 346–352 (2012).
37. Otsuki, T. et al. Genetic and biological characterization of human myeloma cell lines: An overview of the lines established at Kawasaki Medical School. *Gene Funct. Dis.* **1**, 48–56 (2000).
38. Yang, C.-Y. et al. Engineering chimeric antigen receptor T cells against immune checkpoint inhibitors PD-1/PD-L1 for treating pancreatic cancer. *Mol. Ther. Oncolytics* **17**, 571–585 (2020).
39. Hidalgo, M. et al. Patient derived xenograft models: an emerging platform for translational cancer research. *Cancer Discov.* **4**, 998–1013 (2014).
40. Du, H. et al. Antitumor responses in the absence of toxicity in solid tumors by targeting B7-H3 via chimeric antigen receptor T cells. *Cancer Cell* **35**, 221–237.e228 (2019).
41. Tantalò, D. G. et al. Understanding T cell phenotype for the design of effective chimeric antigen receptor T cell therapies. *J. Immunother. Cancer* **9**, e002555 (2021).
42. Bulliard, Y., Andersson, B. S., Baysal, M. A., Damiano, J. & Tsimberidou, A. M. Reprogramming T cell differentiation and exhaustion in CAR-T cell therapy. *J. Hematol. Oncol.* **16**, 108 (2023).
43. Alizadeh, D. et al. IL15 enhances CAR-T-cell antitumor activity by reducing mTORC1 activity and preserving their stem cell memory phenotype. *Cancer Immunol. Res.* **7**, 759–772 (2019).
44. Arcangeli, S. et al. CAR T cell manufacturing from naive/stem memory T lymphocytes enhances antitumor responses while curtailing cytokine release syndrome. *J. Clin. Investig.* **132**, e150807 (2022).
45. Giavridis, T. et al. CAR T cell-induced cytokine release syndrome is mediated by macrophages and abated by IL-1 blockade. *Nat. Med.* **24**, 731–738 (2018).
46. Hong, S. et al. Optimizing dendritic cell vaccine for immunotherapy in multiple myeloma: tumour lysates are more potent tumour antigens than idiotype protein to promote anti-tumour immunity. *Clin. Exp. Immunol.* **170**, 167–177 (2012).
47. Vanderkerken, K., Asosingh, K., Croucher, P. & Van Camp, B. Multiple myeloma biology: lessons from the 5TMM models. *Immunol. Rev.* **194**, 196–206 (2003).
48. Ueland, T. et al. Dickkopf-1 enhances inflammatory interaction between platelets and endothelial cells and shows increased expression in atherosclerosis. *Arterioscler Thromb. Vasc. Biol.* **29**, 1228–1234 (2009).
49. Zagami, P. & Carey, L. A. Triple negative breast cancer: Pitfalls and progress. *npj Breast Cancer* **8**, 1–10 (2022).
50. Wall, J. A., Klempner, S. J. & Arend, R. C. The anti-DKK1 antibody DKN-01 as an immunomodulatory combination partner for the treatment of cancer. *Expert Opin. Investig. Drugs* **29**, 639–644 (2020).
51. June, C. H., O’Connor, R. S., Kawalekar, O. U., Ghassemi, S. & Milone, M. C. CAR T cell immunotherapy for human cancer. *Science* **359**, 1361–1365 (2018).
52. Yu, B., Jiang, T. & Liu, D. BCMA-targeted immunotherapy for multiple myeloma. *J. Hematol. Oncol.* **13**, 125 (2020).
53. Park, J. H., Geyer, M. B. & Brentjens, R. J. CD19-targeted CAR T-cell therapeutics for hematologic malignancies: interpreting clinical outcomes to date. *Blood* **127**, 3312–3320 (2016).
54. Wu, Y. et al. A new immunotherapy strategy targeted CD30 in peripheral T-cell lymphomas: CAR-modified T-cell therapy based on CD30 mAb. *Cancer Gene Ther.* **29**, 167–177 (2022).
55. Niu, Z. et al. CAR-based immunotherapy for breast cancer: peculiarities, ongoing investigations, and future strategies. *Front. Immunol.* **15**, 1385571 (2024).
56. Li, X., Zhao, L., Li, W., Gao, P. & Zhang, N. HER2-targeting CAR-T cells show highly efficient anti-tumor activity against glioblastoma both in vitro and in vivo. *Genes Immun.* **25**, 201–208 (2024).
57. Botta, G. P. et al. Metastatic gastric cancer target lesion complete response with Claudin18.2-CAR T cells. *J. Immunother. Cancer* **12**, e007927 (2024).
58. Uslu U., June C. H. Beyond the blood: expanding CAR T cell therapy to solid tumors. *Nature Biotechnol.* **43**, 506–515 (2024).
59. Han, X., Wang, Y., Wei, J. & Han, W. Multi-antigen-targeted chimeric antigen receptor T cells for cancer therapy. *J. Hematol. Oncol.* **12**, 128 (2019).
60. Hirabayashi, K. et al. Dual-targeting CAR-T cells with optimal co-stimulation and metabolic fitness enhance antitumor activity and prevent escape in solid tumors. *Nat. Cancer* **2**, 904–918 (2021).
61. Gebhardt, T., Park, S. L. & Parish, I. A. Stem-like exhausted and memory CD8+ T cells in cancer. *Nat. Rev. Cancer* **23**, 780–798 (2023).
62. Gattinoni, L., Speiser, D. E., Lichterfeld, M. & Bonini, C. T memory stem cells in health and disease. *Nat. Med.* **23**, 18–27 (2017).

63. Ghorashian, S. et al. Enhanced CAR T cell expansion and prolonged persistence in pediatric patients with ALL treated with a low-affinity CD19 CAR. *Nat. Med.* **25**, 1408–1414 (2019).
64. Shabaneh, T. B. et al. Systemically administered low-affinity HER2 CAR T cells mediate antitumor efficacy without toxicity. *J. Immunother. Cancer* **12**, e008566 (2024).
65. Olson, M. L. et al. Low-affinity CAR T cells exhibit reduced trogocytosis, preventing rapid antigen loss, and increasing CAR T cell expansion. *Leukemia* **36**, 1943–1946 (2022).
66. Jaschke, N. P. et al. Dickkopf1 fuels inflammatory cytokine responses. *Commun. Biol.* **5**, 1391 (2022).
67. Liu, L. et al. Enhanced CAR-T activity against established tumors by polarizing human T cells to secrete interleukin-9. *Nat. Commun.* **11**, 5902 (2020).
68. Ma, X. et al. CD36-mediated ferroptosis dampens intratumoral CD8+ T cell effector function and impairs their antitumor ability. *Cell Metab.* **33**, 1001–1012.e1005 (2021).
69. Sun, F. et al. Bispecific BCMA/CD24 CAR-T cells control multiple myeloma growth. *Nat. Commun.* **15**, 615 (2024).
70. Ma, X. et al. Cholesterol induces CD8+ T cell exhaustion in the tumor microenvironment. *Cell Metab.* **30**, 143–156.e145 (2019).
71. Qian, J. et al. Targeting heat shock proteins for immunotherapy in multiple myeloma: generation of myeloma-specific CTLs using dendritic cells pulsed with tumor-derived gp96. *Clin. Cancer Res. Off. J. Am. Assoc. Cancer Res.* **11**, 8808–8815 (2005).
72. Hong, B. et al. p38 MAPK inhibits breast cancer metastasis through regulation of stromal expansion. *Int. J. Cancer* **136**, 34–43 (2015).
73. Sakamaki, I. et al. Lenalidomide enhances the protective effect of a therapeutic vaccine and reverses immune suppression in mice bearing established lymphomas. *Leukemia* **28**, 329–337 (2014).
74. Knudsen, E. S. et al. Pancreatic cancer cell lines as patient-derived avatars: genetic characterisation and functional utility. *Gut* **67**, 508–520 (2018).
75. Zhang, L. et al. B-cell lymphoma patient-derived xenograft models enable drug discovery and are a platform for personalized therapy. *Clin. Cancer Res.* **23**, 4212–4223 (2017).
76. Xian, M. et al. Leukocyte immunoglobulin-like receptor B1 (LILRB1) protects human multiple myeloma cells from ferroptosis by maintaining cholesterol homeostasis. *Nat. Commun.* **15**, 5767 (2024).

## Acknowledgements

This work was supported by Startup Support from Houston Methodist Research Institute, Houston Methodist Hospital, by Cancer Prevention & Research Institute of Texas Recruitment of Established Investigator Award (RR180044) and High-Impact/High-Risk Research Award (RP210868), and by Leukemia and Lymphoma Society Translational Award (#6682-24) to Q.Y. Q.Y. and his research group were also supported by NCI R01s (CA239255, CA282099, CA278787, CA2855209, and CA285203 to Q.Y.). The authors thank the Houston Methodist Research Institute Research Pathology Core for histological studies, the Comparative Medicine Program for supporting animal studies, and the Flow Cytometry Core for flow cytometry studies.

## Author contributions

Conceptualization, Q.Y., J.Q., W.X., and Y.Z.; Methodology, Y.Z., W.X., J.Q., and Q.Y.; Investigation, Y.Z., W.X., J.Q., R.D., Q.G., Q.W., L.Z., W.W., C.Z., Y.L., L.X., and M.X.; Writing: Y.Z., W.X., and Q.Y.; Funding acquisition, Q.Y.; Resources, J.Q. and Q.Y.; Clinical collaborators: J.C.C. and N.F.E.; Critical reading and suggestion: Y.L., N.F.E., L.Z., and J.C.C.; Supervision: J.Q. and Q.Y.

## Competing interests

J.Q., W.X., and Q.Y. are inventors on patents in the field of DKK1-A2 targeted Therapies. The remaining authors declare no competing financial interests.

## Additional information

**Supplementary information** The online version contains supplementary material available at <https://doi.org/10.1038/s41467-026-69621-8>.

**Correspondence** and requests for materials should be addressed to Liuling Xiao, Ling Zhong or Qing Yi.

**Peer review information** *Nature Communications* thanks Maria-Angela Aznar-Gomez, Akira Kikuchi, Paola Dama and Raymond Liu for their contribution to the peer review of this work. A peer review file is available.

**Reprints and permissions information** is available at <http://www.nature.com/reprints>

**Publisher's note** Springer Nature remains neutral with regard to jurisdictional claims in published maps and institutional affiliations.

**Open Access** This article is licensed under a Creative Commons Attribution-NonCommercial-NoDerivatives 4.0 International License, which permits any non-commercial use, sharing, distribution and reproduction in any medium or format, as long as you give appropriate credit to the original author(s) and the source, provide a link to the Creative Commons licence, and indicate if you modified the licensed material. You do not have permission under this licence to share adapted material derived from this article or parts of it. The images or other third party material in this article are included in the article's Creative Commons licence, unless indicated otherwise in a credit line to the material. If material is not included in the article's Creative Commons licence and your intended use is not permitted by statutory regulation or exceeds the permitted use, you will need to obtain permission directly from the copyright holder. To view a copy of this licence, visit <http://creativecommons.org/licenses/by-nc-nd/4.0/>.

© The Author(s) 2026